ELSEVIER

Lithos 64 (2002) 97–130

LITHOS

www.elsevier.com/locate/lithos

Crystal fractionation in the petrogenesis of an alkali monzodiorite–syenite series: the Oshurkovo plutonic sheeted complex, Transbaikalia, Russia☆

Boris A. Litvinovsky[a,b,*], Bor-ming Jahn[c], Ada N. Zanvilevich[b], Michael G. Shadaev[a]

[a] *Geological Institute, Russian Academy of Sciencies, Ulan-Ude, Russia*
[b] *Ben-Gurion University of Negev, P.O. Box 653, Beer-Sheva 84105, Israel*
[c] *Geosciences Rennes, Universite de Rennes 1, 35042 Rennes Cedex, France*

Received 29 June 2001; accepted 21 June 2002

Abstract

The Oshurkovo Complex is a plutonic sheeted complex which represents numerous successive magmatic injections into an expanding system of subparallel and subvertical fractures. It comprises a wide range of rock types including alkali monzodiorite, monzonite, plagioclase-bearing and alkali-feldspar syenites, in the proportion of about 70% mafic rocks to 30% syenite. We suggest that the variation within the complex originated mainly by fractional crystallization of a tephrite magma.

The mafic rocks are considered as plutonic equivalents of lamprophyres. They exhibit a high abundance of ternary feldspar and apatite, the latter may attain 7–8 vol.% in monzodiorite. Ternary feldspar is also abundant in the syenites. The entire rock series is characterized by high Ba and Sr concentrations in the bulk rock samples (3000–7000 ppm) and in feldspars (up to 1 wt.%). The mafic magma had amphibole at the liquidus at 1010–1030 °C based on amphibole geothermometer. Temperatures as low as this were due to high H_2O and P_2O_5 contents in the melt (up to 4–6 and ~2 wt.%, respectively). Crystallization of the syenitic magmas began at about 850 °C (based on ternary feldspar thermometry). The series was formed at an oxygen fugacity from the NNO to HM buffer, or even higher.

The evolution of the alkali monzodiorite–syenite series by fractional crystallization of a tephritic magma is established on the basis of geological, mineralogical, geochemical and Sm–Nd and Rb–Sr isotope data. The geochemical modeling suggests that fractionation of amphibole with subordinate apatite from the tephrite magma leaves about 73 wt.% of the residual monzonite melt. Further extraction of amphibole and plagioclase with minor apatite and Fe–Ti oxides could bring to formation of a syenite residuum. Rb–Sr isotopic analyses of biotite, apatite and whole-rock samples constrain the minimum age of basic intrusions at ca. 130 Ma and that of cross-cutting granite pegmatites at ca. 120 Ma. Hence the entire evolution took place in an interval of ≤10 My. Initial $^{87}Sr/^{86}Sr$ ratios for the mafic rocks range from 0.70511 to 0.70514, and for syenites from 0.70525 to 0.70542. Initial ε_{Nd} (130 Ma) values for mafic rocks vary from −1.9 to −2.4, and for syenites from −2.9 to −3.5. In a $\varepsilon_{Nd}(T)$ vs. $(^{87}Sr/^{86}Sr)_i$ diagram, all rock types of the complex fall in the enriched portion of the Mantle Array, suggesting their derivation from a metasomatized mantle source. However, the small but distinguishable

☆ Electronic supplements available on the journal's homepage: http://www.elsevier.com/locate/lithos.

* Corresponding author. Ben-Gurion University of Negev, P.O. Box 653, Beer-Sheva 84105, Israel. Tel.: +972-8-6477519.
E-mail address: borisl@bgumail.bgu.ac.il (B.A. Litvinovsky).

PII: S0024-4937(02)00179-2

difference in Sr and Nd isotopic compositions between mafic rocks and syenites probably resulted from mild (10–20%) crustal contamination during differentiation. Large negative Nb anomalies are interpreted as a characteristic feature of the source region produced by Precambrian fluid metasomatism above a subduction zone rather than by crustal contamination.

Keywords: Oshurkovo sheeted intrusion; Tephrite magma; Alkali monzodiorite; Syenite; Fractional crystallization; Sr–Nd isotopes

1. Introduction

A variety of models have been suggested to explain the generation of syenite magmas. These models may be divided into three groups. Models in the first group suggest that syenite magmas may form by melting of crustal rocks during an influx of volatiles (Allen and Chappell, 1992; Lubala et al., 1994) or in a closed system at pressures typical of the base of an overthickened crust (Huang and Wyllie, 1981). The second group of models regards syenite magmas as products of partial melting of metasomatized mantle (Sutcliffe et al., 1990; Lynch et al., 1993) or as residual melts formed by differentiation of alkali basalt magma (Parker, 1983; Brown and Becker, 1986; Thorpe and Tindle, 1992). The third group comprises magma mixing processes, particularly mixing of basic and silicic melts with subsequent differentiation of the resulting hybrid liquids (Barker et al., 1975; Sheppard, 1995; Zhao et al., 1995; Litvinovsky et al., 1999), or mixing of mantle-derived, silica-undersaturated alkaline magmas with granitic magmas formed by melting of lower crustal material above a zone of mafic underplating (Dorais, 1990).

This range of petrogenetic models may reflect the diversity of geological settings in which syenite magmas are generated. In this context, it is important to study in detail plutonic complexes in which the dominance of one particular mechanism of syenite magma production may be established with confidence. The Oshurkovo Intrusive Complex in Transbaikalia, Russia, which is composed of a continuous alkali monzodiorite-to-syenite series, is an appropriate case. In this paper, we present petrographic, mineral chemical, geochemical and Sr–Nd isotopic data from these rocks and demonstrate that the syenite magmas were mainly formed as a result of crystal fractionation from a parental tephritic magma although with some assimilation of crustal silicic material.

2. Geology

2.1. Regional setting

The Oshurkovo Intrusive Complex is situated in South Siberia, near Lake Baikal, in the lower reaches of the Selenga River, about 10 km north–west from the city of Ulan-Ude (Fig. 1). It was extensively studied in the 1960s due to its contained apatite deposit. The complex was considered as a dioritic pluton intruded by a granite magma in the Late Riphean, and subjected to intensive metasomatism accompanied by apatitization (Kuznetsov, 1980 and references therein). Our investigations during 1996–1998 have resulted in a considerable revision of these concepts (Litvinovsky et al., 1998). It was shown that the intrusive complex called the Oshurkovo Massif is of Early Cretaceous age and is made up of rocks of the monzodiorite–syenite series. The Early Cretaceous is one of the main stages of intracontinental rifting that preceded the last rift stage, the Baikal Rift formation in South Siberia (Zanvilevich et al., 1985; Wickham et al., 1995; Yarmolyuk et al., 1995, 1998). During the Early Cretaceous, large volumes of alkali basalts, with subordinate trachytes, phonolites and tephrites filled numerous depressions throughout the Transbaikalian territory, within a geodynamic environment similar to that of the Province of Basins and Ranges (Yarmolyuk et al., 1998).

The Oshurkovo Intrusive Complex forms an irregular intrusive body trending roughly N–S, with a dimension of 5.5×3.5 km . Alluvial deposits of the Selenga River cover its eastern margin (Fig. 1). The intrusive body is distinctly discordant with respect to the surrounding gneisses and gneissic granites, presumably of Late Riphean age. Abundant tectonic breccia and strong mylonitization along the northern margin of the complex suggest the presence of an E–W oriented fault. The complex is made up of alkali

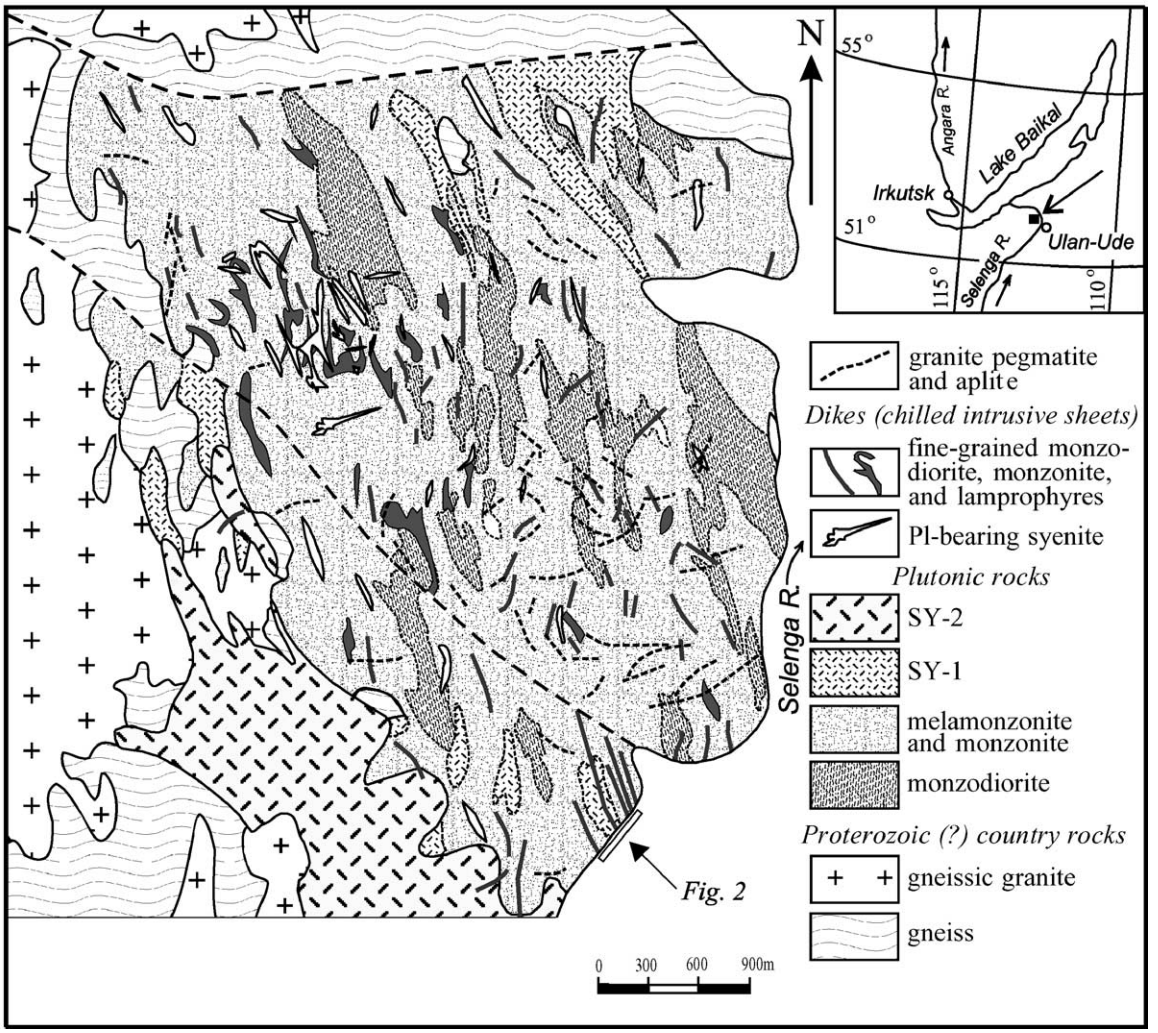

Fig. 1. Geological sketch map of the Oshurkovo Complex, compiled with the use of authors' and Kuznetsovs' (1980) data. In the index map (inset) the arrow indicates the location of the complex.

monzodiorite and monzonite (70%) and subordinate syenite (30%). Two main stages of intrusion can be distinguished: an early monzodiorite–syenite stage involving the formation of a magmatic series from alkali monzodiorite to plagioclase-bearing syenite (SY-1), and a late-stage intrusion of alkali-feldspar syenite (SY-2). The latter forms several irregular bodies, the largest of which is located in the southern part of the complex (Fig. 1).

The Oshurkovo Complex is composed of numerous steeply dipping conformable bodies of lenticular, tabular, or dike-like morphology; xenoliths or screens of the country rocks are extremely rare. The bodies range from a few hundred meters to 2 km in length and from 2–3 to 600 m in width. They are oriented NNW 340°, with steep dips from 70° to 90°. Fig. 2 shows a sketch of a cross-section seen in a road-cut in the southern part of the complex (see location in Fig. 1). Twenty individual bodies of coarse- to medium-grained monzodiorite, monzonite, syenite, and numerous fine-grained dikes were found within a 350-m interval. Each mafic body is composed of only one rock type. Contacts between the plutonic bodies are sharp and planar (Fig. 3A). Evidence of thermal

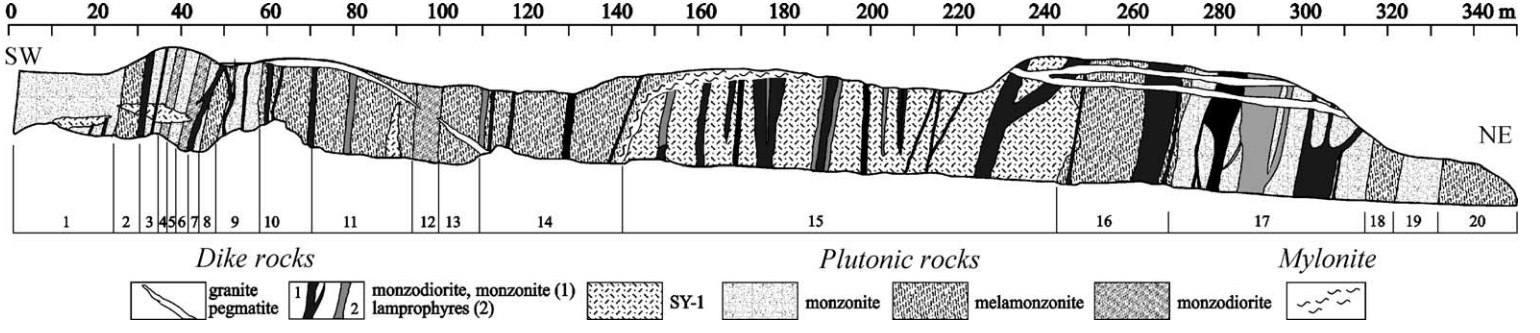

Fig. 2. Alternation of subvertical monzodiorite, monzonite and syenite intrusive bodies and chilled intrusive sheets (dikes). Sketch of the road-cut in the southern part of the Oshurkovo Complex. The plutonic bodies are numbered consecutively, as shown below the sketch. The vertical scale is two times the horizontal.

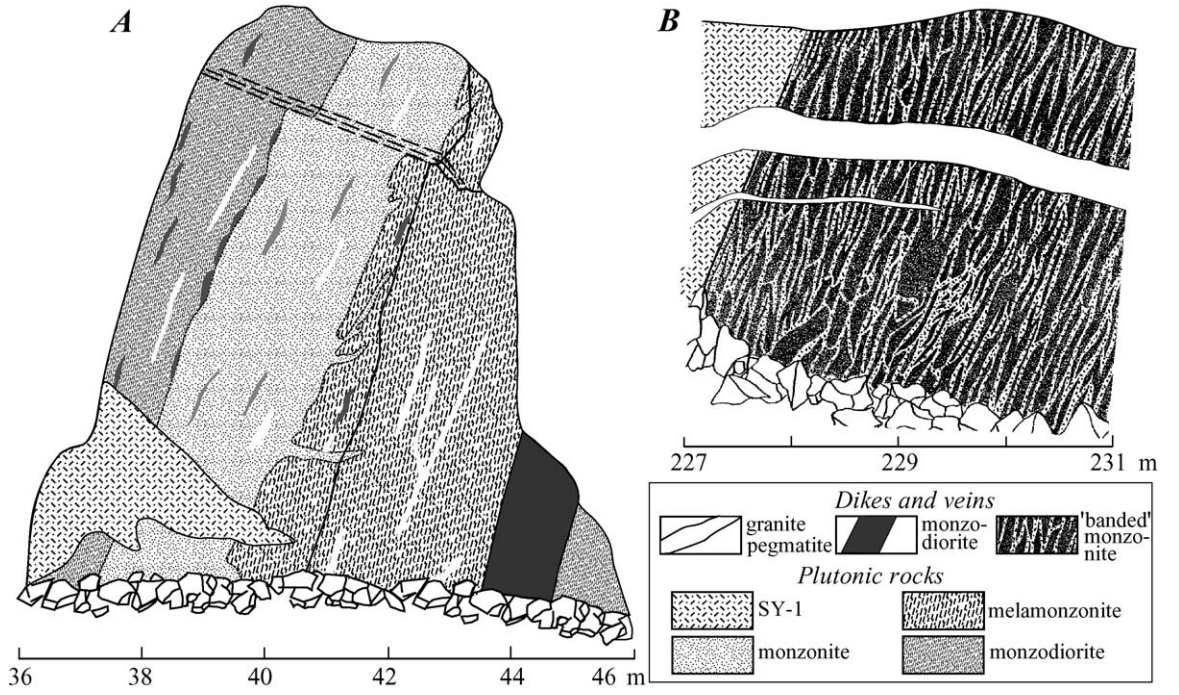

Fig. 3. Structure of plutonic bodies and banded dike. (A) Alternating conformable near-vertical monzodiorite and monzonite bodies with numerous light and dark elongated lenses. In the lower left part of the outcrop is a fragment of a subhorizontal cutting intrusive syenite body. (B) Banded dike consisting of extended melamonzonite lenses and light monzonitic and syenitic veins. The distances below the sketches correspond to the scale and position of the outcrop in Fig. 2.

effects in the contact zones in particular decrease of grain size is extremely rare, although thin vein-like apophyses can be distinguished in places (Fig. 3A). This suggests that the intrusive pulses were separated by short time intervals, and the injection of each subsequent magma occurred before the earlier magma was completely crystallized and cooled. Despite a considerable range in silica content in the Oshurkovo rocks, there is no apparent temporal trend in the compositional variation of successive magmas (from basic to silicic or reverse). Injections of syenite magma alternated with mafic magma, although syenite emplacement was more abundant during the later stages of complex formation. Consequently, the Oshurkovo Complex has an unusual structure similar to that of an ophiolite sheeted dike complex, and it may be regarded as a plutonic sheeted complex. Its structure is described in more details elsewhere (Litvinovsky et al., 1998).

A characteristic feature of the Oshurkovo Complex is the presence of hundreds of dike-like bodies made up of fine-grained to porphyritic rocks, commonly with chilled margins (only a small part of these bodies is shown in Fig. 1). These bodies make up about 10% of the complex. Compositionally, they are similar to the plutonic rocks and range from alkali monzodiorite and lamprophyre to syenite and alkali-feldspar syenite. Injections of mafic and syenitic magma that formed the dike-like bodies followed irregularly upon each other, as during the plutonic stages. However, the youngest dikes are mafic rather than syenitic. Most of them, like the coarse-grained plutonic bodies, also show NNW orientation and are steeply dipping; not infrequently they are commensurable in size to the plutonic bodies (Figs. 2 and 3). We interprete the dike-like bodies as chilled intrusive sheets timed to the final stages of formation of the complex.

One more special feature of the Oshurkovo Complex is the abundance of monzonitic and syenitic pegmatites. They form segregations within the plutonic bodies and, more frequently, veins or networks of veins

cross-cutting these bodies. In places they are intersected by basic and syenitic dikes. The youngest intrusive rocks are the numerous granitic pegmatite and aplite veins.

From a detailed analysis of the structure of the complex and contact relationships between the plutonic bodies, Litvinovsky et al. (1998) concluded that the present-day position of the Oshurkovo Complex corresponds to its initial orientation, i.e. it cannot be regarded as a layered sill-like body, tilted later by tectonic processes.

2.2. Internal structure in the alkali mafic rocks

In spite of their small size, individual monzodiorite and monzonite bodies often exhibit structural heterogeneity. Banding in some bodies resembles layering, but the bands are in fact elongated lenses with contrasting mafic/felsic mineral proportions. The lenses are from a few tens of centimetres to 1.5 m long and from 3–4 to 20 cm wide, oriented conformably to the margins. The leucocratic lenses range in composition from monzonite to syenite due to enrichment in the feldspar constituents. More common are irregularly intercalated light and dark lense-like segregations aligned conformably with the host plutonic body (Fig. 3A). They are made up of rocks with typical magmatic textures, without any signs of recrystallization and tectonic deformation.

Heterogeneities are also observed in some of the larger dike-like bodies. Mostly, it is exhibited in regularly alternating bands and strongly elongated pods (Fig. 3B). The dark pods are made up of fine-grained monzodiorite and melamonzonite (SiO_2 = 44.5–47.8 wt.%) while the lighter bands consist of fine-grained monzonite (SiO_2 = 49.5 wt.%); in places their composition ranges to syenite (SiO_2 = 58 wt.%, K_2O = 4–6 wt.%). The banding is always conformable with the strike and dip of dikes, and it is observed either throughout the whole dike or in its marginal sections only. Rarely, composite dikes formed by mingling of melanocratic and leucocratic mafic magmas or of mafic and syenitic magmas are observed. The mafic enclaves are of oval shape and have crenulated, sinuous, lobate contours and chilled margins, showing evidence of ductile deformation. These features of the composite dikes are similar to features described by Wiebe (1973), Vogel and Wilband (1978) and Reid and Hamilton (1987).

Some mafic plutonic bodies and chilled intrusive sheets contain highly melanocratic inclusions, which are irregular in shape, vary in size from 20–30 cm to a few metres, and have gradational contacts with the host rock. They consist mainly of euhedral amphibole, rare pyroxene crystals (together up to 60–65 vol.%) and apatite (10–12 vol.%); subordinate feldspars and minor biotite form interstitial phases. Random arrangement of such inclusions within the host bodies and orientation parallel to steeply dipping boundaries suggest that the inclusions are disrupted fragments of cumulates that were transported by mafic magma from deeper levels.

3. Analytical procedures

3.1. Mineralogy

Microprobe analyses were carried out on polished thin sections using a four-channel MAR-3 electron

Table 1
Average modal composition of main rock types from the Oshurkovo Complex

Rock type	Amphibole	Biotite	Pyroxene	Plagioclase (An < 50)	Ternary feldspar	Alkali feldspar	Apatite	Opaque, accessor
Monzodiorite (MD)	34	4	3	30	11	2	7	7
Melamonzonite (MM)	26	12	2	25	22	2	5	6
Monzonite (M)	13	12		28	34	6	3	4
Plagioclase bearing syenite (SY-1)	9	4	2	20	22	43	2	1
Alkali feldspar syenite (SY-2)	1	2	2			94	< 1	< 1

microprobe at Geological Institute, Russian Academy of Sciences, Ulan-Ude, with WDS Detector system and a beam diameter of 2–3 μm. Operating conditions were 20 kV, 40 μA beam current, with 10 s counting time. To determine the bulk compositions of ternary feldspar and alkali feldspar, crystals were scanned, and bulk compositions were estimated from total counts/time. Cryptoperthitic and microperthitic ternary feldspar and alkali feldspar analyses are averages obtained by traversing regularly exsolved regions of about 50–60 μm at a rate of 30 μm/min, whereas for perthitic crystals the scanning rate was increased to 100 μm/min, and analyses represent bulk compositions obtained by traversing, mostly from margin to margin. The detection limits are 0.05–0.09 wt.% for Na_2O, MgO, Al_2O_3, and SiO_2; 0.01–0.05 wt.% for Cl, K_2O, CaO, TiO_2, MnO, and FeO; 0.06–0.15 wt.% for BaO; 0.3–0.4 wt.% for SrO and F; 0.1–0.2 wt.% for REE. Mineral name abbreviations are according to Kretz (1983). Total iron and FeO in biotite were determined in order to estimate oxygen fugacity. Biotites were separated from all main rock types and analysed by atomic absorption spectrometry (total iron) and titration (FeO).

Table 2
Microprobe analyses (wt.%) of amphiboles in representative rock types of the Oshurkovo Complex. A complete data set is available on the journal's homepage: http://www.elsevier.com/locate/lithos under "Electronic Supplements"

Sample no.	38-3^T	58^T	64	58-4^T	61^{T,M}	34-1^M	58-1	24-5	24-1	36-1	35-2
	CUM	MD		MM		M	SY-1	SY-2		Mafic dikes	
SiO_2	41.58	40.37	40.89	39.31	40.45	40.70	41.12	44.27	49.47	40.95	40.92
TiO_2	4.24	4.8	3.79	4.9	4.12	3.51	2.85	1.9	0.89	3.73	3.25
Al_2O_3	11.66	11.63	11.98	11.62	11.55	11.83	11.33	8.69	5.35	11.42	10.85
FeO	12.63	13.2	13.96	13.28	14.81	15.87	15.21	17.92	15.55	14.44	14.94
MnO	0.17	0.18	0.17	0.17	0.17	0.21	0.24	0.52	0.37	0.21	0.26
MgO	12.14	11.63	11.37	11.65	10.94	10.51	11.14	10.5	13.09	10.78	11.43
CaO	11.32	11.19	11.35	11.12	11.35	11.45	11.27	10.52	10.43	11.44	10.97
Na_2O	2.43	2.42	2.56	2.36	2.37	2.29	2.27	2.53	2.51	2.49	2.47
K_2O	1.79	1.78	1.71	1.66	1.86	1.93	1.72	1.59	0.78	1.63	1.94
Cl	n.d.	0.03	0.03	0.02	0.05	n.d.	0.06	0.22	0.08	–	n.d.
F	n.d.	0.67	0.27	0.62	0.57	n.d.	0.72	1.19	0.95	0.74	n.d.
	97.96	97.9	98.08	96.71	98.24	98.3	97.93	99.85	99.47	97.83	97.03
O=F, Cl		0.29	0.12	0.27	0.25		0.32	0.55	0.42	0.31	
Total	97.96	97.61	97.96	96.44	97.99	98.3	97.61	99.3	99.05	97.52	97.03
Atoms to 23 oxygens and 13 cations in (T+C) sites											
Si	6.191	6.088	6.137	5.991	6.115	6.125	6.206	6.614	7.204	6.224	6.193
Al_{iv}	1.809	1.912	1.863	2.009	1.885	1.875	1.794	1.386	0.796	1.776	1.807
Al_{vi}	0.236	0.153	0.254	0.077	0.172	0.221	0.220	0.143	0.121	0.268	0.127
Ti	0.475	0.544	0.428	0.562	0.469	0.397	0.324	0.214	0.097	0.426	0.370
Fe^{3+}		0.004	0.030	0.157	0.046	0.129	0.287	0.412	0.371		0.283
Mg	2.695	2.615	2.544	2.647	2.466	2.358	2.506	2.339	2.842	2.443	2.579
Fe^{2+}	1.573	1.661	1.722	1.536	1.827	1.868	1.633	1.827	1.522	1.836	1.608
Mn	0.021	0.023	0.022	0.022	0.022	0.027	0.031	0.066	0.046	0.027	0.033
Ca_B	1.806	1.808	1.825	1.816	1.838	1.846	1.822	1.684	1.627	1.863	1.779
Na_B	0.194	0.192	0.175.	0.184	1.162	0.154	0.178	0.316	0.373	0.137	0.221
Na_A	0.508	0.516	0.570	0.513	0.533	0.514	0.487	0.417	0.336	0.597	0.504
K_A	0.340	0.342	0.327	0.323	0.359	0.371	0.331	0.303	0.145	0.316	0.375
Sum A	0.848	0.858	0.897	0.836	0.892	0.885	0.818	0.72	0.481	0.913	0.879

(1) Abbreviations as in Table 1.
(2) Samples marked with superscripts "T" and "M" were used for determination of crystallization temperature and for geochemical modelling, respectively.
(3) Here and in Tables 3–6, n.d. = not determined; symbol "–" = below detection limit.
(4) The analyses are selected points.

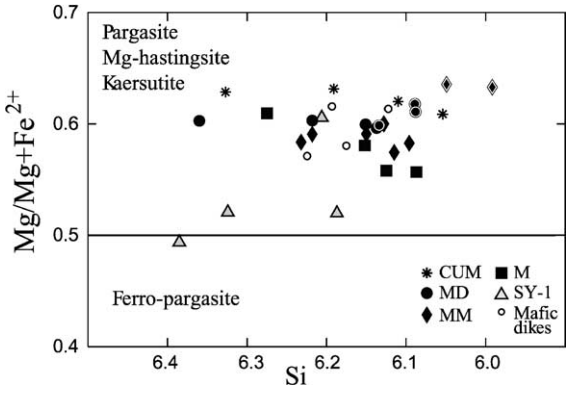

Fig. 4. Si vs. $Mg/Mg+Fe^{2+}$ plot for amphiboles (after Leake, 1978). CUM = cumulates, MD = monzodiorite, MM = melamonzonite, M = monzonite, SY-1 = early Pl-bearing syenite, SY-2 = late alkali feldspat syenite. Rimmed symbols denote kaersutites.

3.2. Geochemistry

All analyses were made using a combination of wet chemical methods, AAS and titration (major elements), X-ray fluorescence (Rb, Sr, Ba, Y, Zr, Nb, and Th) and atomic emission spectrometry (Co, Cr, Ni, and V) at the Geological Institute, Ulan-Ude. Rare-earth elements were determined mainly by instrumental neutron activation at the Analytical Center of Geological Institute, Moscow; several samples were analyzed by ICP-MS at the CRPG-CNRS, Nancy. Analyses are considered accurate to within 2–5% for major elements, and better than 10–15% for trace elements. The accuracy for all the REE (except Lu) is 1–5%, for Lu 9–10%. Normalized trace-element concentrations were calculated with respect to chondrite and primitive mantle (Sun and Mc Donough, 1989).

3.3. Rb–Sr and Sm–Nd isotopes

The isotope ratios were measured at the Universite de Rennes, France (Rb–Sr and Sm–Nd) and at the Geological Institute, Ulan-Ude (Rb–Sr). The analytical techniques at Rennes can be found in Jahn et al. (1996). Mass analyses were performed using a seven-collector Finnigan MAT-262 mass spectrometer in static mode for Sr and dynamic mode for Nd. $^{87}Sr/^{86}Sr$ ratios were normalized against the value of $^{86}Sr/^{88}Sr = 0.1194$. Long-term replicate analyses (>150) on NBS-987 Sr standard yielded $^{87}Sr/^{86}Sr = 0.710259 \pm 5$ (2σ). $^{143}Nd/^{144}Nd$ ratios were normalized against the value of $^{146}Nd/^{144}Nd = 0.7219$. Long-term replicate analyses (>150) on an in-house (Rennes) Ames Nd standard gave $^{143}Nd/^{144}Nd = 0.511966 \pm 5$ (2σ), which is equivalent to the La Jolla Nd standard of 0.511860. At the Geological Institute the Rb and Sr isotope ratios were measured on a MI-1201 T mass spectrometer, and the mean $^{87}Sr/^{86}Sr$ ratios for the VNIIM standard is 0.707988.

The notations of ε_{Nd} and $f_{Sm/Nd}$ are defined according to common equations (Faure, 1986). Isochron ages were calculated using the regression program ISOPLOT (Ludwig, 1999). Input errors are 2% for $^{87}Rb/^{86}Sr$, 0.005% for $^{87}Sr/^{86}Sr$. Unless specified, the errors quoted in ages represent $\pm 2\sigma$ is enough.

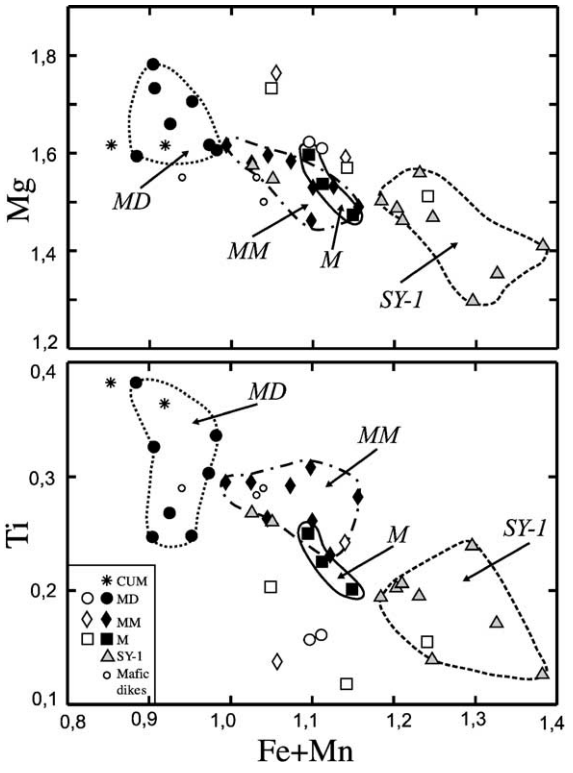

Fig. 5. (Fe + Mn) vs. Ti and (Fe + Mn) vs. Mg diagrams for biotites. In the right column symbols and abbreviations as in Fig. 4; in the left column symbols denote biotite from late Cpx–Bt assemblages.

4. Petrography

4.1. Mafic plutonic rocks

Mafic rocks constitute the greatest part of the complex. They are dark, medium- to coarse-grained, rarely porphyritic, mostly homogenous, but in places with clear intercalation of darker and lighter stripes. Rocks in the stripes do not exhibit evidence of lamination. Three main types of mafic rocks are distinguished: monzodiorite, melamonzonite and monzonite (Table 1). In melamonzonite, the color index is slightly less than those recommended by IUGS for melanocratic rocks, but we have made this subdivision because two distinct varieties of monzonite are clearly recognized and compose discrete plutonic bodies.

Monzodiorite and melamonzonite are very similar in texture and mineral composition despite different proportion of mafic and felsic minerals (Table 1). In both rock types, brown pargasite/hastingsite, occasionally kaersutite, are the dominant mafic minerals. Amphibole usually forms euhedral grains and is rarely zoned. Corroded grains of early augite, frequently enclosed in amphibole, were found in some bodies.

Table 3
Microprobe analyses and wet chemical iron determinations (wt.%) of biotites in representative rock types of the Oshurkovo Complex. A complete data set is available on the journal's homepage: http://www.elsevier.com/locate/lithos under "Electronic Supplements"

Sample no.	38-3	64	54-5^{L}	61	8^{L}	34-1	54-10^{L}	9	2	57-1	33-1	36-1	53-10	39-5	65-1
	CUM	MD		MM		M		SY-1		SY-2		Mafic dikes		Dike-SY1	Dike-SY2
SiO_2	35.95	36.50	36.97	36.18	37.32	36.68	36.61	36.89	36.39	36.93	38.10	37.11	36.12	38.82	37.33
TiO_2	6.57	5.31	2.81	5.34	2.88	3.50	3.47	3.35	2.93	2.99	3.51	5.16	5.04	1.79	3.50
Al_2O_3	14.35	13.26	13.44	13.53	12.53	14.16	13.34	13.06	13.43	12.57	10.43	13.30	13.15	12.87	11.96
FeO*	14.62	15.22	17.20	17.01	16.59	17.94	16.41	19.33	20.15	18.09	18.93	14.68	15.92	15.80	16.91
MnO	0.12	0.13	0.19	0.19	0.14	0.13	0.16	0.08	0.26	0.22	0.17	0.12	0.19	0.29	0.19
MgO	14.55	14.31	14.14	12.84	15.55	13.04	15.38	13.79	11.68	13.8	13.19	13.74	12.99	14.72	14.14
CaO	0.00	0.09	0.00	0.00	0.05	0.00	0.00	0.08	0.04	0.04	0.00	0.00	0.00	0.10	0.16
Na_2O	0.20	0.23	0.21	0.00	0.14	0.17	0.12	0.11	0.12	0.09	0.06	0.16	0.18	0.10	0.13
K_2O	9.79	9.76	9.75	9.47	10.31	10.09	10.33	9.68	9.45	9.98	10.42	9.35	9.53	99.44	9.72
Cl	n.d.	0.07	n.d.	0.10	0.12	n.d.	n.d.	n.d.	0.20	n.d.	n.d.	0.09	n.d.	0.08	0.35
F	n.d.	1.16	n.d.	1.20	2.08	1.09	n.d.	n.d.	0.78	1.58	1.30	1.35	1.02	1.68	1.05
		96.04		95.87	96.58	96.80			95.43	96.29	96.10	95.06	94.17	95.69	95.44
O=F, Cl		0.51		0.54	0.92	0.47			0.38	0.68	0.56	0.60	0.44	0.73	0.72
Total	96.15	95.52	94.71	95.33	96.66	96.33	95.82	96.37	95.05	95.61	95.54	94.46	93.73	94.96	94.72
Atoms to 11 oxygens															
Si	2.679	2.766	2.825	2.763	2.830	2.785	2.767	2.797	2.827	2.842	2.946	2.810	2.790	2.950	2.876
Al iv	1.260	1.185	1.175	1.218	1.121	1.215	1.188	1.167	1.173	1.140	0.951	1.190	1.200	1.050	1.086
Ti iv	0.061	0.049		0.019	0.055		0.045	0.036		0.018	0.103		0.010		0.038
Al iv			0.035			0.053			0.056					0.100	
Ti vi	0.304	0.253	0.161	0.288	0.060	0.201	0.153	0.155	0.171	0.155	0.101	0.290	0.280	0.100	0.165
Fe	0.911	0.965	1.099	1.086	1.053	1.141	1.038	1.226	1.309	1.640	1.224	0.930	1.030	1.000	1.089
Mn	0.008	0.008	0.012	0.012	0.009	0.008	0.011	0.005	0.017	0.014	0.011	0.010	0.010	0.020	0.012
Mg	1.616	1.617	1.610	1.462	1.759	1.474	1.733	1.559	1.353	1.583	1.520	1.550	1.500	1.670	1.624
Ca	0.000	0.007	0.000	0.000	0.004	0.000	0.000	0.006	0.003	0.003	0.000	0.000	0.000	0.000	0.013
Na	0.029	0.034	0.031	0.026	0.021	0.026	0.015	0.016	0.018	0.013	0.009	0.020	0.030	0.010	0.019
K	0.931	0.944	0.950	0.923	0.998	0.978	0.996	0.937	0.936	0.980	1.028	0.900	0.940	0.920	0.955
Wet chemical determinations of FeO and FeO; Fe_2O_3 by differences*															
Fe_2O_3	3.33	3.64		6.98		5.44		7.49	9.39	7.06	9.95			9.35	10.39
FeO	11.06	11.59		12.41		12.89		13.16	12.69	12.68	9.50			10.83	7.56
FeO*	14.06	14.87		18.69		17.79		19.90	21.14	19.03	18.46			19.25	16.91

(1) Abbreviations as in Table 1.
(2) Samples marked with superscript "L"=biotite from the late Cpx–Bt assemblages.

Table 4
Microprobe analyses (wt.%) of pyroxenes in representative rock types of the Oshurkovo Complex

Sample no.	38-3	37-1	54-5^{L}	34-7	32-1^{L}	9	51-11	57-5	5	35-1
	Cumulate (CUM)	Monzodiorite (MD)		Melamonzonite (MM)		SY-1		SY-2	Mafic dikes	
SiO_2	50.91	50.69	53.04	50.38	51.87	50.65	52.60	52.47	50.23	51.11
TiO_2	0.83	0.84	0.05	0.84	0.08	0.67	0.15	0.34	0.86	0.51
Al_2O_3	3.55	3.26	0.93	3.23	1.26	2.87	1.31	1.19	3.18	2.05
FeO*	9.35	9.14	9.16	9.79	9.32	10.89	11.13	12.41	8.94	9.31
MnO	0.25	0.26	0.33	0.24	0.28	0.29	0.38	0.40	0.24	0.36
MgO	13.03	12.03	12.61	12.08	13.34	12.09	11.46	11.18	12.46	12.80
CaO	21.22	21.38	22.04	21.75	22.93	21.57	21.82	19.89	22.06	22.37
Na_2O	1.05	1.31	1.29	1.45	0.95	1.63	1.53	2.19	1.52	1.26
K_2O	0.03	0.06	0.03	0.01	0.01	0.02	0.00	0.02	0.03	0.03
Total	100.23	98.97	99.48	99.77	100.02	100.65	100.38	100.09	99.52	99.80
Atoms to 6 oxygens and 4 cations										
Si	1.886	1.904	1.982	1.877	1.926	1.873	1.961	1.960	1.898	1.929
Al iv	0.114	0.096	0.018	0.123	0.054	0.124	0.039	0.040	0.142	0.091
Al vi	0.040	0.048	0.023	0.019	0.000	0.002	0.018	0.012	0.040	0.020
Ti	0.023	0.024	0.001	0.024	0.020	0.023	0.004	0.010	0.024	0.015
Fe^{3+}	0.104	0.098	0.088	0.161	0.142	0.202	0.123	0.168	0.185	0.162
Fe^{2+}	0.186	0.189	0.198	0.144	0.131	0.127	0.224	0.219	0.091	0.114
Mn	0.008	0.008	0.010	0.008	0.009	0.009	0.012	0.013	0.008	0.012
Mg	0.720	0.674	0.702	0.671	0.738	0.667	0.637	0.623	0.701	0.721
Ca	0.842	0.860	0.882	0.868	0.912	0.855	0.871	0.796	0.892	0.905
Na	0.075	0.095	0.093	0.105	0.068	0.117	0.111	0.159	0.111	0.092
K	0.002	0.003	0.001		0.000	0.001		0.001	0.001	0.002

(1) SY-1 = early Pl-bearing syenite, SY-2 = late alkali feldspar syenite.
(2) Samples marked with superscript "L" = pyroxene from the late Cpx–Bt assemblages.

Bright reddish-brown plates and flakes of minor unzoned biotite are always present. Feldspars are mainly plagioclase (25–28% An) and ternary feldspar, both forming either equant, tabular or anhedral interstitial grains. Minor alkali feldspar is always interstitial. Apatite is abundant and amounts to up to 7–8%. Apatite grains occur as inclusions in the early amphibole, or closely associate with late minerals (biotite and feldspars). This points to a wide temperature interval for apatite crystallization. Accessories are idiomorphic and isometrical grains of ilmenite and titanomagnetite, with rare titanite.

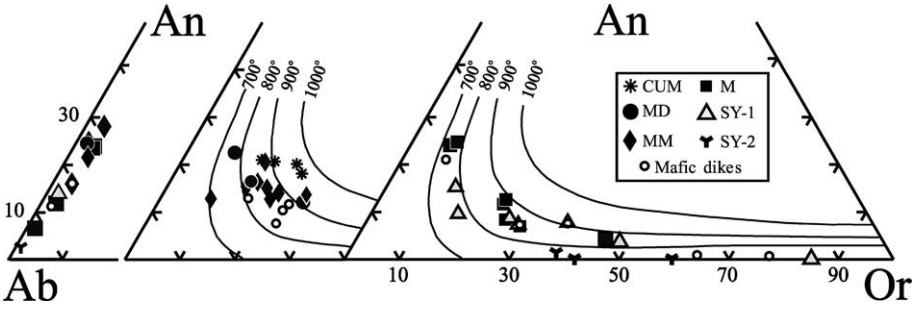

Fig. 6. Feldspar compositions plotted in the An–Ab–Or diagrams (in mol%). The solvus isotherms at $P = 5$ kbar are from Nekvasil (1992). Symbols as in Fig. 4.

In *monzonite*, the dominant minerals are feldspars: microperthtic ternary feldspar, twinned plagioclase (25% An) and perthite. Cryptoperthitic tabular crystals, rarely with a plagioclase core, are common. The amount of perthite grains is noticeably higher than in the more melanocratic varieties, up to 5–7 vol.%. Biotite and amphibole (pargasite, Mg-hastingsite) are present in equal proportion, while early augite is extremely rare. Apatite contents are about 3%; accessory minerals are Fe–Ti oxides, titanite and rare allanite.

In some mafic rocks late clinopyroxene and biotite are found. These minerals are present as separate grains and flakes or as rims around early amphibole and biotite. The proportion of late mafic minerals ranges from a few to 15 vol.%. As a rule, rocks with

Table 5
Microprobe analyses (wt.%) of ternary feldspar, alkali feldspar and plagioclase in representative rock types of the Oshurkovo Complex. A complete data set is available on the journal's homepage: http://www.elsevier.com/locate/lithos under "Electronic Supplements"

Sample no.	38-3	59	37-1	32-1	34-7		54-10	34-1	32-11^{M}
	CUM	MD		MM			M		
SiO_2	60.36	60.24	61.80	62.11	60.92	60.06	63.31	60.43	61.83
TiO_2	0.04	0.16	0.06	n.d.	0.06	0.04	0.06	0.01	0.08
Al_2O_3	22.68	23.77	21.31	22.24	23.05	24.05	21.25	24.06	23.02
FeO*	0.03	0.10	0.15	0.1	0.08	0.10	0.15	n.d.	0.41
MnO	0.04	0.04	0.02	n.d.	0.04	0.04	0.04	0.03	0.05
MgO	n.d.	n.d.	0.05	n.d.	0.02	0.01	0.01	n.d.	n.d.
CaO	3.62	5.13	2.35	2.53	4.08	5.72	1.73	4.98	3.60
Na_2O	6.48	7.65	6.89	7.38	7.03	7.53	7.57	7.85	8.83
K_2O	3.90	0.87	4.50	3.35	2.53	0.59	4.30	1.27	0.28
BaO	0.97	0.17	0.73	0.84	1.09	0.43	0.79	0.30	0.18
SrO	1.89	0.89	1.54	1.31	0.61	0.64	0.78	1.38	1.19
Total	100.01	99.02	99.40	99.86	99.51	99.21	99.99	100.34	99.47
An	18.1	25.6	12.1	12.8	20.6	28.5	8.4	24.1	18.1
Ab	58.7	69.2	61.5	67.2	64.2	68.0	66.7	68.6	80.2
Or	23.2	5.2	26.4	20	15.2	3.5	24.9	7.3	1.7
Number of analyses	1	1	1	2	2	2	3	2	1

Sample no.	68-1	7	9		57-1	31-13	35-2	I-2-1	65-1
	M	SY-1			SY-2	Mafic dikes			Dike-SY2
SiO_2	62.95	63.22	60.53	64.82	64.17	62.04	62.46	61.54	65.89
TiO_2	0.06	0.06	0.01	n.d.	0.02	0.08	0.04	0.06	0.04
Al_2O_3	20.03	19.84	23.09	21.52	19.05	21.80	21.18	22.94	18.75
FeO*	0.10	0.14	0.09	0.08	0.08	0.11	0.13	0.10	0.08
MnO	0.03	0.04	0.05	0.00	0.04	0.04	0.04	0.03	0.02
MgO	0.04	0.04	0.03	0.00	n.d.	0.01	0.03	0.03	0.03
CaO	0.91	0.80	3.11	3.11	0.11	2.60	2.18	4.16	0.58
Na_2O	5.65	5.41	8.19	9.92	4.66	7.87	7.61	7.91	6.16
K_2O	7.76	8.27	2.14	0.39	10.47	2.68	4.11	1.35	8.15
BaO	1.45	0.85	0.69	–	0.52	0.83	0.93	0.30	0.55
SrO	0.65	1.02	1.09	0.42	0.50	1.91	0.63	1.02	0.49
Total	99.63	99.69	99.02	100.26	99.62	99.95	99.33	99.43	100.73
An	4.5	3.9	15.2	14.4	0.6	13.0	10.5	20.7	3.0
Ab	50.2	47.9	72.3	83.4	40.1	71.0	66.0	71.2	51.5
Or	45.3	48.2	12.4	2.2	59.3	16.0	23.5	8.0	45.5
Number of analyses	1	1	1	1	5	2	2	2	2

Abbreviations as in Table 1.

a high proportion of the late Cpx + Bt assemblage contain higher amounts of apatite and titanite, and show large interstitial Fe–Ti oxide grains. Judging from the noticeable increase of K_2O in these rocks (see below, Table 7, Fig. 9), formation of alkali feldspar at this stage is also possible.

4.2. Felsic plutonic rocks

Felsic rocks are represented by two main types, plagioclase-bearing syenite of the early stage (SY-1) and alkali feldspar syenite of the late stage (SY-2).

Syenite of the early stage is similar in appearance to monzonite, only distinguished by lighter color and lower content of mafic minerals (Table 1). It is made up mostly of large anhedral grains of perthitic alkali feldspar, with lesser amounts of irregular microperthitic ternary feldspar and tabular albite-oligoclase, infrequently with alkali feldspar rims. Mafic minerals are the same as in the basic rocks. Accessories are apatite (1–2.5%), titanite, Fe–Ti oxides and single small zircon and allanite grains.

Alkali-feldspar syenite is medium- to coarse-grained, occasionally porphyritic. Mafic minerals (biotite, edenite and salite) comprise 3–7 vol.%. It is made up predominantly of alkali feldspar with distinct vein perthites. Quartz is usually absent, although in places patches of quartz-bearing syenite with 8–12% quartz are found. Accessory minerals are titanite, magnetite, apatite (up to 1%), and zircon.

4.3. Rocks of the dike-like bodies (chilled intrusive sheets)

Dike-like bodies are made up of rock types similar in mineral compositions to their plutonic counterparts. Felsic rocks are equigranular, fine- to medium-grained. Mafic rocks are fine-grained equigranular or porphyritic. Among the porphyritic rocks, lamprophyres (kersantite and spessartite) are abundant. In lamprophyres, the phenocryst assemblage is Prg + Ap + Bt ± Aug; matrix (50–90 vol.%) consists of the same minerals as well as plagioclase (An_{28-30}), ternary feldspar and alkali feldspar. Porphyritic varieties of monzodiorite and monzonite differ from lamprophyres in the presence of plagioclase phenocrysts and higher (>20 vol.%) total proportion of phenocrysts. In many mafic dikes late Cpx + Bt assemblage is also distinguished; in places it is accompanied by noticeable amounts of titanite.

5. Mineral chemistry

In Tables 2–6, data on mineral chemistry are given. A complete set of analyses for Tables 2, 3, 5

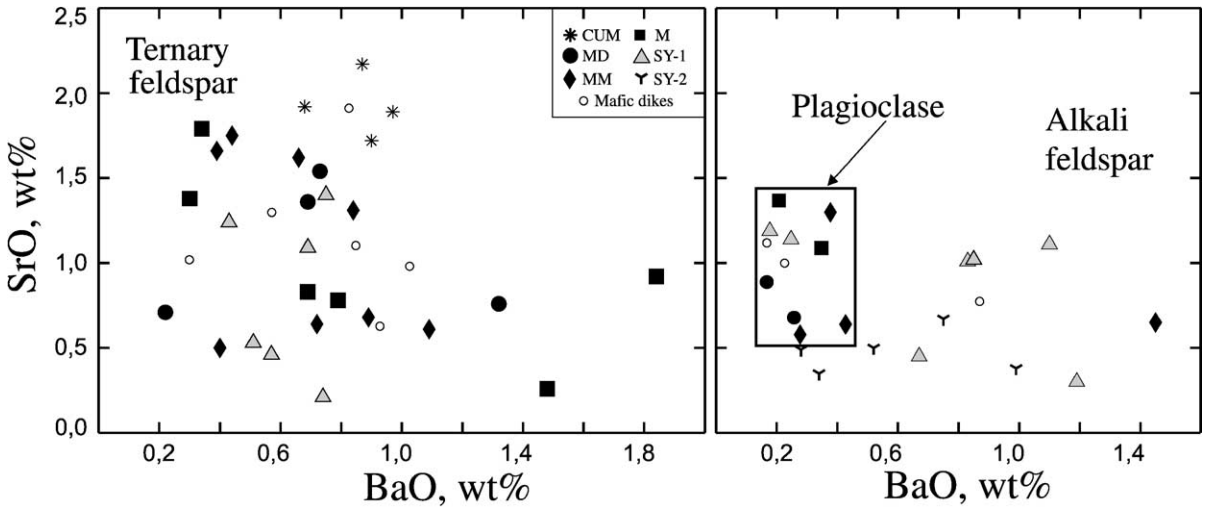

Fig. 7. Compositions of ternary feldspar, plagioclase and alkali feldspar in the rocks of the Oshurkovo Complex plotted in BaO vs. SrO diagrams. Symbols and abbreviation as in Fig. 4.

and 6 may be found on the journal's website at http://www.elsevier.com/locate/lithos under "Electronic Supplements".

Amphibole in the monzodiorite–syenite series, according to Leake (1978), is pargasite–hastingsite (Ca_B>1.7; Na_A+K_A>0.7; Si=5.99–6.38 apfu); in SY-2 it is edenite and hornblende (Table 2). In the classification diagram (Fig. 4) compositions of amphiboles from mafic rocks overlap almost completely; however, kaersutite was observed only in monzodiorite and melamonzonite. Amphiboles from SY-1 are characterized by lower $Mg/Mg+Fe^{2+}$ value and decreased Ti contents (Table 2, Fig. 4). The distinctive feature of amphiboles for all types of rocks is the high contents of K_2O, from 1.6 to 2 wt.%, TiO_2, >2.5%, and F, ~ 0.5 wt.% in amphibole from mafic rocks to 1.19 wt.% in amphibole from SY-2 (Table 2).

Biotite is ubiquitous in both mafic and felsic rocks, even though it is not present in large amounts. In all types of rocks it corresponds to annite–phlogopite (after Rieder et al., 1999), with high contents of TiO_2 (3.0–6.8 wt.%) and F (0.8–1.4 wt.%). In Mg vs. (Fe+Mn) and Ti vs. (Fe+Mn) plots (Fig. 5) biotite compositions from various rocks partly overlap; at the same time, the tendency of decreasing Mg and Ti is accompanied by an increase in (Fe+Mn) from monzodiorite to syenite. Biotite from late Cpx+Bt assemblage in all types of mafic rocks contains more Mg and less Ti than early biotite (Table 3, Fig. 5).

Clinopyroxene in the mafic rocks have a limited chemical variation, although some distinction between pyroxenes of two different populations can be seen. The early pyroxene always fall in the augite field on the criteria of Deer et al. (1978) while late pyroxene is salite that contains less Ti and Al (Table 4). Pyroxenes from syenite are similar in composition both to early and late pyroxenes from monzodiorite–monzonite (Table 4), but in syenite there is no evidence for its two-stage crystallization.

Feldspars in mafic and felsic rocks are plagioclase, alkali feldspar and ternary feldspar. After Ribbe (1983), ternary feldspar is defined here as feldspar that contains more than 5 mol% Ab, An and Or. In monzodiorite, melamonzonite and cumulates, ternary feldspar is richer in An than in some but not all monzonite and syenite (Fig. 6, Table 5). Plagioclase in mafic rocks and in syenite contains 2–4% Or and only 15–30% An (Table 5). Alkali feldspar is characterized by a fairly narrow range of Ab molar content (40–60%), whereas the An proportion attains 3.9% (Table 5). A distinctive feature of feldspars from the Oshurkovo Complex is the enhanced Ba and Sr concentrations. Fig. 7 shows that both plagioclase and alkali feldspar are enriched in BaO and SrO. In plagioclase, BaO content is up to 0.4 wt.%, with 1.3 wt.% SrO, while in alkali feldspar both BaO and SrO contents attain 1.1 wt.%. High Ba and Sr concentrations, up to 1.5 wt.% BaO and 2.0 wt.% SrO,

Table 6
Microprobe analyses (wt.%) of apatites in representative rock types of the Oshurkovo Complex. A complete data set is available on the journal's homepage: http://www.elsevier.com/locate/lithos under "Electronic Supplements"

Sample no.	38-3	$11a^M$	54-10	2	54-12
	CUM	MM	M	SY-1	Mafic dike
SiO_2	0.34	0.35	0.36	0.33	0.59
FeO*	0.10	0.15	0.06	0.07	0.08
MnO	0.10	0.10	0.09	0.09	0.11
MgO	0.07	0.05	0.04	0.04	0.06
CaO	53.30	52.93	53.75	54.49	52.93
Na_2O	0.27	0.28	0.18	0.18	0.41
P_2O_5	40.51	39.82	40.35	40.48	39.75
SrO	0.49	1.09	0.44	0.35	0.52
SO_3	0.73	–	0.53	0.49	0.85
F	3.81	4.56	3.26	3.37	3.16
Cl	0.20	0.1	0.09	0.08	0.12
La_2O_3	0.10	0.23	–	–	0.21
Ce_2O_3	0.24	0.47	0.23	0.18	0.59
Nd_2O_3	0.18	0.31	0.15	0.07	0.36
	100.43	100.45	99.53	100.24	99.71
O=F, Cl	1.65	1.98	1.39	1.44	1.36
Total	98.78	98.47	98.14	98.80	98.35
Atoms to 12 oxygens					
P	2.814	2.585	2.813	2.806	2.774
S	0.045		0.033	0.030	0.052
Si	0.028	0.027	0.030	0.027	0.049
Fe	0.007	0.010	0.004	0.005	0.005
Mn	0.007	0.007	0.006	0.006	0.008
Mg	0.008	0.006	0.006	0.005	0.007
Ca	4.685	4.349	4.742	4.780	4.675
Na	0.042	0.042	0.029	0.028	0.065
Sr	0.023	0.048	0.021	0.017	0.025
La	0.003	0.006			0.006
Ce	0.007	0.013	0.007	0.005	0.018
Nd	0.005	0.008	0.004	0.002	0.011
F	0.988	1.107	0.849	0.873	0.825
Cl	0.027	0.012	0.013	0.012	0.016
Number of analyses	1	1	3	9	1

Abbreviations as in Table 1.

Table 7
Major (wt.%) and trace element (ppm) compositions of representative samples of the plutonic rocks, selected dikes and country-rock gneissic granite

Sample no.	38-3	58-3	58	59	37-1	64	151-1[L]	61	11a
	Cumulate (CUM)		Monzodiorite (MD)					Melamonzonite (MM)	
SiO_2	41.70	42.40	40.20	41.50	44.00	44.20	43.50	46.54	46.94
TiO_2	3.20	3.35	4.76	4.31	3.24	3.11	3.17	3.09	2.80
Al_2O_3	11.90	14.23	13.30	14.20	13.10	13.70	13.60	16.12	16.30
Fe_2O_3	5.82	5.57	4.55	4.46	5.98	3.47	2.45	4.68	4.53
FeO	3.82	4.27	7.26	7.20	4.21	6.83	6.61	5.59	6.04
MnO	0.10	0.08	0.12	0.07	0.09	0.10	0.10	0.09	0.07
MgO	6.00	7.40	7.69	6.61	7.10	6.56	6.38	4.51	4.66
CaO	15.20	11.20	10.65	10.60	12.20	10.54	10.20	6.83	7.50
Na_2O	3.15	3.24	3.05	3.31	3.32	3.23	2.92	4.48	4.44
K_2O	1.85	2.55	1.97	1.93	2.39	2.65	3.96	3.26	2.79
P_2O_5	4.50	4.06	3.13	3.22	2.79	3.04	3.35	1.65	1.67
LOI	2.54	1.60	2.90	2.09	1.26	2.15	3.40	2.72	1.77
Total	99.78	99.95	99.58	99.50	99.68	99.58	99.64	99.56	99.51
ne(Q)	5.4	3.5	4.3	3.4	6.1	3.4	6.4	5.8	5.0
Rb	19	11	10	17	11	14	28	28	19
Ba	2700	3300	3400	3000	3200	5000	8110	6000	5800
Sr	5300	8200	5700	5800	5100	6600	7220	7600	9000
Zr	100	95	120	120	130	110	260	120	92
Nb	4	6	3	6	5	6	7	6	2
Y	19	23	28	25	24	19	28	15	21
Cr	68	36	32	27	120	69	n.d.	18	47
Ni	110	98	100	70	160	82	n.d.	30	70
Co	31	50	41	32	50	36	n.d.	30	62
V	190	220	220	250	240	210	n.d.	230	200

Sample no.	40-4	9[M]	7	24-1	33-1	57-1	14	79-5	51-7
	Early syenite (SY-1)			Late syenite (SY-2)			QSY-2	Monzon. pegmatite	
SiO_2	55.00	56.40	56.90	63.00	62.00	62.80	66.24	58.5	60.3
TiO_2	1.60	1.37	1.29	0.45	0.87	0.32	0.48	0.52	1.23
Al_2O_3	17.70	18.28	17.75	18.70	18.10	18.50	16.1	17.2	17.3
Fe_2O_3	4.20	2.73	3.19	1.01	2.41	2.62	1.69	0.99	1.72
FeO	2.62	2.80	2.11	1.22	2.04	0.92	1.29	2.55	2.04
MnO	0.04	0.04	0.04	0.02	0.03	0.02	0.03	0.07	0.04
MgO	1.87	1.97	1.28	0.42	0.84	0.31	0.63	2.64	1.05
CaO	3.71	3.64	4.42	1.16	1.14	0.14	0.62	6.2	3.07
Na_2O	5.09	5.28	5.13	6.10	5.69	5.68	5.34	4.87	4.67
K_2O	5.51	4.95	4.99	6.95	6.34	7.57	6.19	4.37	6.55
P_2O_5	0.53	0.60	0.56	0.13	0.21	0.12	0.23	0.17	0.55
LOI	1.89	1.86	2.43	0.93	0.52	0.49	1.34	1.48	1.02
Total	99.76	99.92	100.09	100.09	100.19	99.49	100.18	99.56	99.54
ne(Q)	3.9	0.9	0.1	1.8	(1.3)	0.01	(9.76)	0.2	(2.4)
Rb	47	46	43	72	78	91	119.6	25	49
Ba	7900	7000	6600	6900	6800	4900	3081	7230	8050
Sr	8890	8050	9300	4450	4300	3800	2444	8000	6410
Zr	78	123	180	73	160	78	290	78	460
Nb	9	7	3	8	6	3	17	n.d.	4
Y	12	12	7	9	10	2	9.0	10	7
Cr	n.d.	8	11	n.d.	5	15	n.d.	73	42
Ni	n.d.	26	25	n.d.	13	17	n.d.	20	15
Co	n.d.	24	15	n.d.	10	7	3.4	16	6.6
V	n.d.	108	150	n.d.	110	110	28.5	100	110

36-2	34-7	32-1^{L}	7a	68-1	32-11^{M}	54-10^{L}	51-11	65	73-3	1
			Monzonite (M)				Early syenite (SY-1)			
44.85	47.90	45.20	49.50	53.00	53.45	47.20	54.00	54.20	54.40	54.60
3.08	2.51	3.13	2.54	1.97	1.61	2.71	1.71	1.93	1.64	1.38
15.05	15.85	14.70	16.50	16.85	17.90	14.70	16.60	16.55	17.80	18.00
4.57	3.84	3.97	3.26	3.01	3.07	5.18	4.19	3.24	3.13	2.52
6.51	5.01	6.56	5.84	4.45	4.13	5.46	2.58	4.09	3.61	3.19
0.09	0.07	0.06	0.07	0.09	0.05	0.08	0.07	0.07	0.06	0.05
5.16	5.28	5.50	3.81	3.38	3.20	4.21	1.69	2.64	2.51	2.13
9.38	8.84	8.79	6.46	5.55	5.40	8.41	5.89	3.97	4.29	4.76
4.28	3.81	3.46	5.04	4.57	5.27	3.89	5.02	4.77	5.40	5.16
2.94	2.87	3.56	3.08	3.94	3.63	3.81	4.27	5.00	3.64	4.23
2.3	2.08	2.54	1.40	1.41	0.97	2.01	0.78	1.24	0.76	1.11
2.12	1.45	2.12	2.04	1.39	1.45	2.40	2.78	1.75	2.20	2.35
100.33	99.51	99.59	99.54	99.61	100.13	100.06	99.58	99.45	99.44	99.48
9.0	1.6	4.6	5.1	–	2.68	5.5	2.4	–	–	0.4
23	7	30	25	28	24	31	28	49	42	56
4400	4500	6000	4800	4900	5300	5800	5700	5800	4900	7200
5900	6000	8300	6500	5200	6500	7300	7100	5300	6300	9600
100	91	110	150	130	62	190	200	62	180	75
11	4	1.0	5	8	7	10	7	5	6	1
17	21	18	14	13	12	21	8	12	6	13
32	80	18	27	27	12	14	21	23	23	16
52	88	76	43	60	23	47	22	50	28	14
50	32	28	32	30	30	26	18	22	38	38
280	240	210	230	160	210	230	210	150	200	160
10	31-13	35-2	35-1	I-2-1	39-4	39-5	25-1	39-1b	65-1	591
Mafic dikes						Dike-SY1	Dike-SY2			GG
42.90	45.00	48.80	48.00	52.45	53.60	56.20	55.60	60.10	62.00	73.02
2.70	3.09	2.25	2.75	1.81	1.61	1.30	1.76	0.62	0.58	0.15
13.90	16.90	14.7	13.7	18.30	16.80	17.40	16.20	18.4	19.00	13.94
7.46	5.25	4.41	2.04	3.72	4.13	3.15	3.29	1.28	1.88	2.00
3.32	4.58	4.99	6.11	4.07	2.54	2.89	3.54	1.75	1.32	
0.11	0.09	0.09	0.08	0.07	0.06	0.05	0.07	0.10	0.02	0.01
5.55	4.82	4.70	7.22	2.68	1.73	1.45	2.87	0.87	0.50	0.22
10.74	8.25	8.28	6.86	4.40	5.62	3.22	3.85	2.57	0.44	0.97
3.55	3.81	3.77	2.77	5.08	4.85	5.19	5.86	5.21	6.00	3.37
3.33	3.73	4.12	5.91	4.70	6.19	6.43	4.01	6.77	6.83	5.66
3.85	2.48	2.07	1.89	0.99	0.91	0.54	1.02	0.36	0.13	0.05
2.12	1.38	1.85	2.17	1.48	2.28	2.17	1.49	1.34	0.81	0.51
99.53	99.38	100.03	99.5	99.74	100.32	99.99	99.56	99.37	99.51	99.90
7.2	6.3	4.0	4.8	4.9	9.0	5.6	1.1	1.0	–	(29.7)
25	17	28	48	28	36	55	77	410	55	204.9
4300	6000	5200	5900	5850	5700	5200	4900	6000	3900	539.8
6000	7900	5400	4600	6145	6090	4930	3910	5660	3100	243.1
210	76	140	280	133	700	500	280	1200	370	136
15	7	9	6	9.5	11	n.d.	10	45	1	12.6
39	20	21	19	18	22	n.d.	11	18	4	8.7
50	45	110	280	16	n.d.	n.d.	n.d.	n.d.	16	n.d.
78	66	89	200	23	n.d.	n.d.	n.d.	n.d.	16	n.d.
32	36	26	25	29	n.d.	n.d.	n.d.	n.d.	10	2.6
180	170	175	160	190	n.d.	n.d.	n.d.	n.d.	74	12.6

Table 8
REE content (ppm) in representative samples of plutonic rocks, selected dike rocks, in apatite, and in country-rock gneissic granite

Sample no.	38	38-3	58-3	59	37-1	34-7	11a^{M}	68-1	32-11^{M}	9^{M}	7	K75-1
	Cumulate (CUM)			Monzodiorite (MD)		Melamonzonite (MM)		Monzonite (M)		Early syenite (SY-1)		
La	95	110	100	85	85	88	93.26	62	60.49	45	50	40
Ce	300	330	310	240	240	240	217.28	150	117.44	98	110	81
Nd	190	200	200	170	160	140	138.36	92	71.9	52	63	36
Sm	25	25	26	20	21	18	21.79	12	11.52	6.2	7.6	5.7
Eu	6.9	7	7.7	5.9	6	5.4	6.56	3.9	4.17	2.9	3.2	2.7
Tb	1.8	1.7	1.8	1.4	1.5	1.2	1.77	0.74	0.95	0.36	0.41	0.28
Yb	1	0.86	0.92	0.78	0.72	0.81	0.75	0.39	0.45	0.29	0.39	0.23
Lu	0.07	0.06	0.05	0.06	0.05	0.06	0.09	0.05	0.07	0.03	0.05	0.04
Eu/Eu*	0.95	0.97	1.03	1.02	0.99	1.04	1.07	1.14	1.28	1.65	1.5	1.71

Sample no.	33-1	57-1	14	31-13	35-1	35-2	I-2-1	65-1	591	38	58-3	11-2
	Late syenite (SY-2)		QSY-2	Mafic dikes				Dike-SY2	GG	Apatite		
La	38	42	62.91	110	71	130	66	47	19.36	830	920	1300
Ce	76	76	129.37	320	170	310	160	93	64.27	2100	2400	3400
Nd	38	24	55.45	190	98	170	89	39	10.45	960	1200	1500
Sm	4.1	3.3	7.17	23	14	23	12	4.2	1.62	140	170	230
Eu	1.7	1.3	1.85	6.7	3.9	5.5	3.7	2.2	0.5	38	44	61
Tb	0.21	0.17	3.52	1.5	0.97	1.3	0.67	0.23	0.23	9.3	9.9	16
Yb	0.36	0.28	0.74	0.59	0.67	0.77	0.57	0.28	1.23	5.6	6.8	9.3
Lu	0.05	0.05	0.11	0.06	0.07	0.1	0.06	0.03	0.21	0.6	0.8	1.1
Eu/Eu*	1.49	1.41	0.91	1.02	0.95	0.85	1.1	1.87	0.95	0.95	0.92	0.93

(1) QSY-2 = alkali feldspar quartz syenite, GG = country-rock gneissic granite. Sample #11-2 = monzonitic pegmatite.
(2) Samples 11a, 32-11, 14 and 591 have been analysed by ICP-MS method. Additional data on the REE content: #11a-Pr = 32.39, Gd = 14.00, Dy = 5.21, Ho = 0.77, Er = 1.57, Tm = 0.13; #32-11-Pr = 17.49, Gd = 7.59, Dy = 2.61, Ho = 0.35, Er = 0.79, Tm = 0.09; #14-Pr = 15.99, Gd = 3.52, Dy = 2.16, Ho = 0.29, Er = 0.86, Tm = 0.12; #591-Pr = 3.46, Gd = 1.28, Dy = 1.12, Ho = 0.27, Er = 0.84, Tm = 0.17.

are also characteristic of the ternary feldspars. The high values for Ba and Sr in feldspars from the Oshurkovo Complex are comparable with those in some alkali gabbro–syenite series, calc–alkaline lamprophyres and basanite–phonolite volcanic suites (Smith and Brown, 1988).

Apatite is a major rock-forming mineral in the mafic rocks (especially the monzodiorite). In some basic dikes it forms abundant phenocrysts. Apatite contains approximately 0.5 wt.% SrO, 3.2–4.4 wt.% fluorine and is classified as fluorapatite (Table 6).

In dikes, feldspars as well as mafic phenocrysts are similar in composition to the rock-forming minerals from plutonic rocks. This is illustrated in a number of plots (Figs. 4–7).

6. Geochemistry

Major- and trace-element data for 40 representative samples of plutonic and dike rocks from the Oshurkovo Complex are reported in Tables 7 and 8. Data for 73 samples are plotted in Fig. 8. It should be stressed that mafic rocks with $\geq 10\%$ late Cpx + Bt assemblage are not included in the discussion because such rocks contain systematically higher CaO, K_2O, P_2O_5, Rb, and lower Al_2O_3, Na_2O than rocks with similar SiO_2 contents in which early mafic minerals (Prg + Bt ± Aug) predominate (Fig. 9). This suggests that formation of late Cpx and Bt occurred under open system conditions at near-solidus or subsolidus temperatures.

Notes to Table 7:
(1) QSY-2 = alkali feldspar quartz syenite, GG = country-rock gneissic granite; ne(Q) = the CIPW normative contents of nepheline (quartz).
(2) Samples marked with superscript "M" were used for geochemical modelling, samples marked with superscript "L" contain >10 vol.% of the late Cpx–Bt assemblages.

The monzodiorite–syenite series ranges continuously in SiO_2 contents from ~40 to 63 wt.%. In almost all rock types normative nepheline is present despite the absence of modal nepheline; the mafic rocks contain up to 9 wt.% normative nepheline (Table 7). This is caused by the high abundances of the low-silica amphibole and biotite in monzodiorite and monzonite. The presence of normative nepheline allows us to call these rocks alkali monzodiorite and alkali monzonite (below the prefix 'alkali' is omitted for brevity). On a TAS plot the Oshurkovo analyses are confined mainly to the tephrite, phono-tephrite, trachyandesite and trachyte fields. This points to rock formation from alkali-rich magmas and suggests that mafic rocks crystallized from tephritic to phono-tephritic magmas.

The most outstanding feature of the Oshurkovo Complex is the unusually high Sr and Ba contents in all the rocks from monzodiorite to alkali-feldspar syenite, and the high contents of P_2O_5, sometimes ≥3%, in the monzodiorite and up to 4.5% in the cumulates (Table 7). This significantly exceeds the contents of Sr, Ba and P_2O_5 from well-known basanite–tephrite localities in the world (e.g. Le Maitre, 1976; Beccaluva et al., 1998), but is comparable with certain calc-alkaline lamprophyres (Rock, 1991).

In the chemical variation diagrams using MgO as the differentiation index (Fig. 8), we have made the following observations: (1) CaO and P_2O_5 correlate positively with MgO for all types of rocks. The correlation is also true for TiO_2, FeO*, and Ni (Table 7), but the trend is not so clear for monzodiorite and

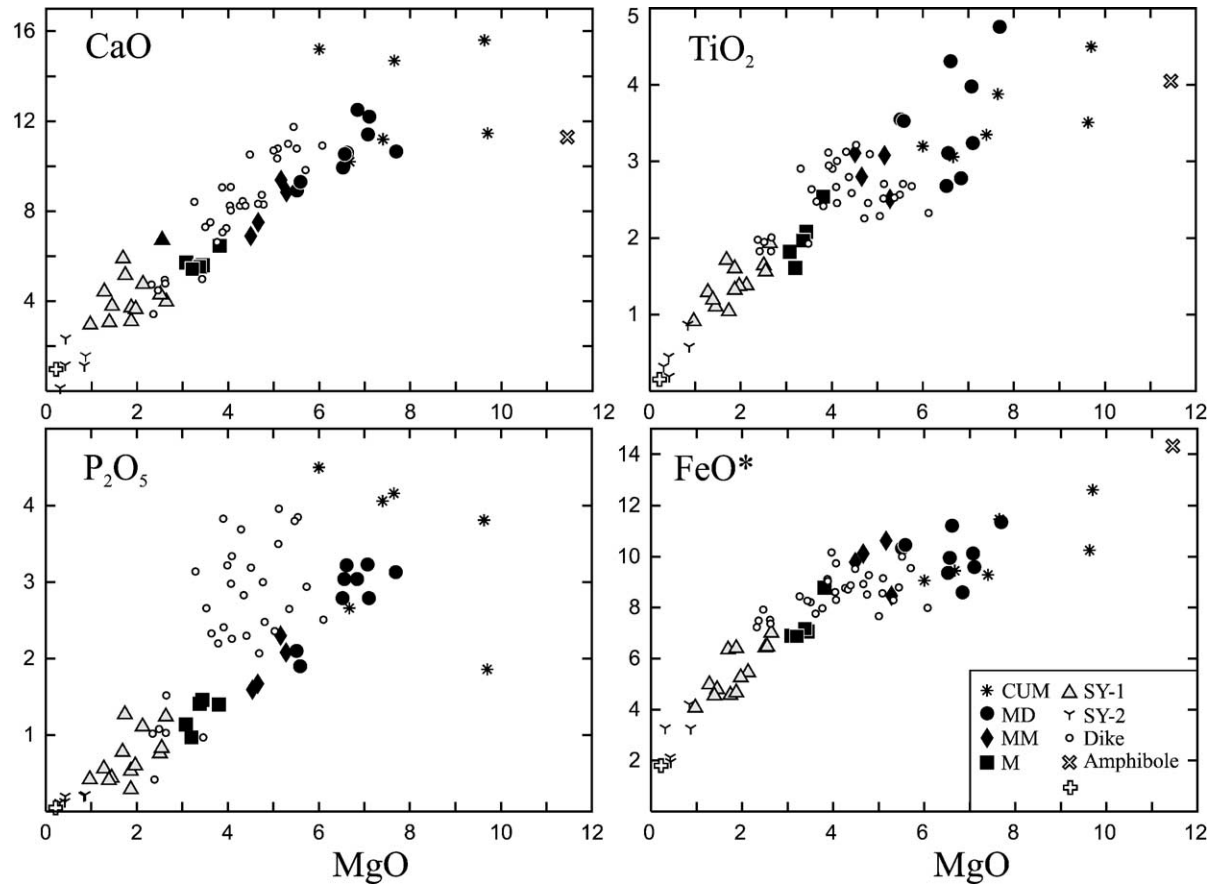

Fig. 8. Chemical variation diagrams for the rocks of the Oshurkovo Complex. Symbols as in Fig. 4. Amphibole = average composition of amphiboles from mafic rocks, GG = country-rock gneissic granite.

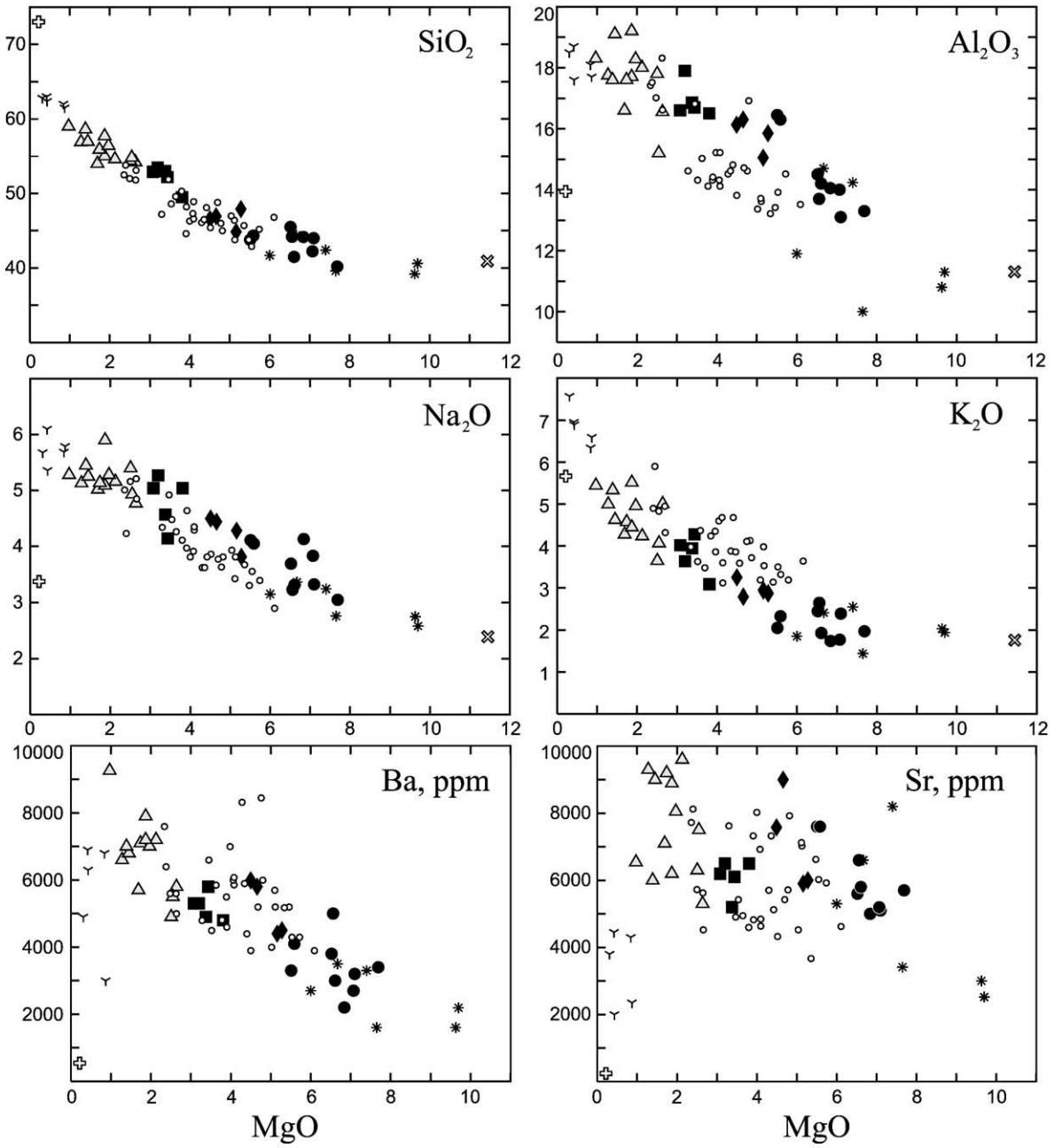

Fig. 8 (*continued*).

melamonzonite. (2) Na_2O and SiO_2 display negative correlation with MgO. Similar behavior is also true for Al_2O_3, K_2O, Rb, and Ba, but within each individual rock type the correlation is unclear or absent. Moreover, in the most evolved SY-2, Ba decreases compared to SY-1. (3) Sr, Zr and Y do not show any correlation with MgO. Their concentrations in mafic rocks and syenite overlap almost totally; only SY-2 has

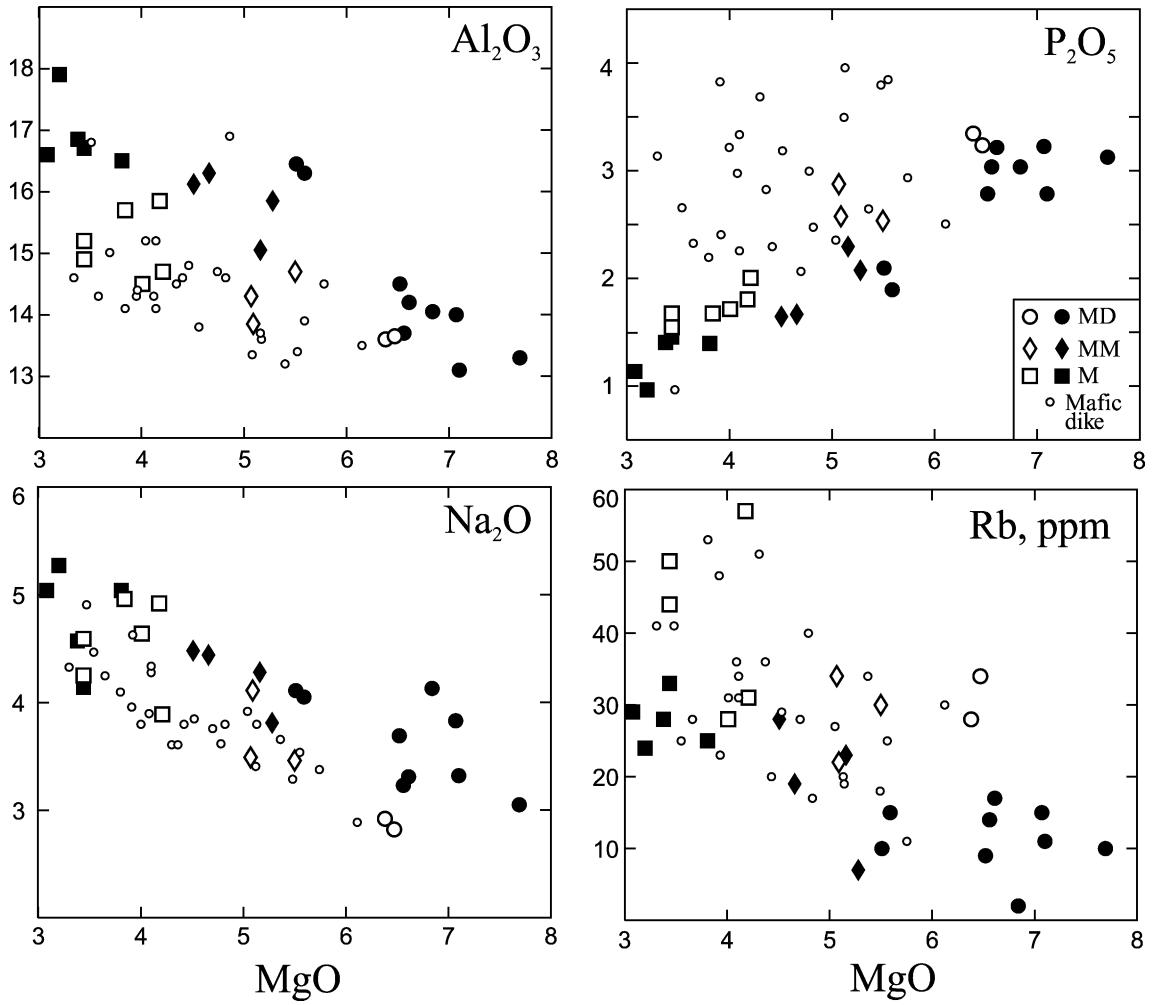

Fig. 9. Chemical variation diagrams for monzodiorite–monzonite group and mafic dikes. Symbols in the left column denote rocks with ≥10 vol.% of late Cpx–Bt assemblages; symbols in the right column as in Fig. 4.

lower Sr content. The correlation of major and trace elements with MgO is consistent with the observed decrease of modal amphibole (±Cpx), along with apatite, and increase of feldspar content from monzodiorite to syenite. The irregular abundance of Sr could be due to the entry of this element into both apatite and feldspar (Tables 5 and 6), so that the modal decrease of apatite was compensated by the modal increase of feldspar in the more leucocratic rocks.

The chemical compositions of dikes, as a whole, are similar to those of the plutonic rocks (Fig. 8), suggesting a close genetic relation between the dikes and the other rocks of the intrusive complex. Slight differences are seen for CaO, Al_2O_3, Na_2O, K_2O, more significant for P_2O_5. Plots in Fig. 9 illustrate that the differences are the same in dikes and in plutonic rocks with marked amounts of late Cpx+Bt assemblage. In the dikes estimation of the proportion of this assemblage is difficult, but the chemical data suggest they contain a significant proportion of late Cpx+Bt.

Fig. 10 shows the rare earth element (REE) distribution patterns in the different rocks of the complex. The total REE content decreases systematically with decreasing contents of the mafic minerals and apatite in the sequence. Since the REE content in apatite is an order of magnitude higher than that in the

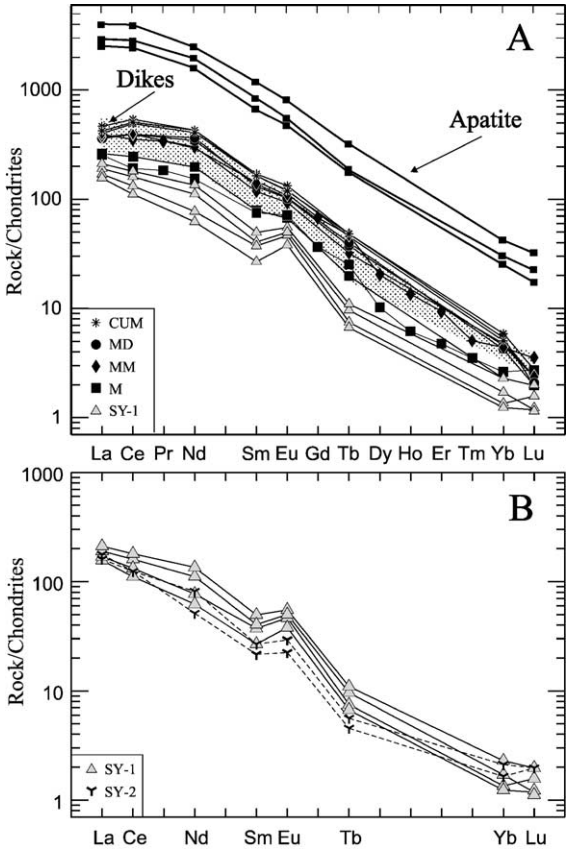

Fig. 10. Chondrite normalized REE patterns of apatite, mafic rocks and syenites of the Oshurkovo Complex. The field of mafic dikes is shown by the stippled area. Symbols as in Fig. 4.

whole-rock samples, it is evident that systematic REE decrease within the sequence is mainly due to decrease in the content of apatite. The Eu anomalies, expressed by Eu/Eu* ratios, increase regularly from monzodiorite (Eu/Eu* = 0.99–1.02) to melamonzonite (1.07) to monzonite (1.14–1.34) and syenite (1.50–1.71) (Table 8). This suggests an increasing contribution from the feldspar component in the rocks.

Primitive-mantle normalized trace element spidergrams shown in Fig. 11 demonstrate similar patterns of element abundances in all main rock types from the series. Both mafic and felsic rocks possess distinct Ba and Sr peaks and deep Nb and Zr troughs. Despite the high TiO_2 content (4.8–2.0% for mafic rocks, ≤ 1.9% for syenites; Table 7), slight negative Ti anomalies are seen in the spidergrams. As a whole, syenitic rocks have higher abundances in all the three most LIL elements—Rb, Ba and K that are characteristic mostly of feldspars.

7. Rb–Sr ages and Sr–Nd isotopes

Rb–Sr and Sm–Nd isotope data for seven whole-rock (WR) samples are given in Table 9. Additional Rb–Sr analyses on WR, biotite, apatite and garnet from granitic and monzonitic pegmatites are also given. The data of biotite–WR or biotite–apatite pairs allow us to estimate the time when biotite cooled to its blocking temperature of about 300 °C (Jäger et al., 1967). Although the blocking temperature depends on many factors that control isotopic and chemical exchange (Jenkin et al., 2001), we will use the concept to constrain the emplacement of the Oshurkovo Complex. For coarse-grained biotites as used in this study, the blocking temperature could be higher than 300 °C.

Fig. 12 shows eight isochron diagrams. A monzodiorite (sampe #59, Fig. 12A) and a cumulate of melanocratic monzodiorite composition (sample #59-1, Fig. 12B) give ages of 126 ± 4 and 135 ± 5 Ma, respectively. These ages are the same within the 2σ error limit. A monzonitic pegmatite (sample #79), which is considered from field relationship to be intruded soon after the plutonic complex formation, has a slightly younger age of 122 ± 8 Ma (Fig. 12C). The entire Oshurkovo Complex was cut by a number of granitic pegmatites which have a tight range of ages about 120 Ma (Fig. 12D, E, F). Their genetic links

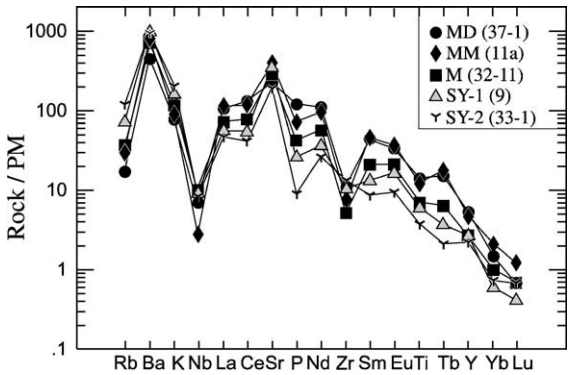

Fig. 11. Primitive mantle-normalized multielement diagrams for monzodiorite–syenite series. Symbols as in Fig. 4; sample numbers as in Table 7.

with the complex are unlikely. Consequently, the biotite ages suggest that the alkali mafic and syenite intrusions took place at about 130 Ma and the granitic pegmatite veins cross-cut them at about 120 Ma. The entire course of magmatic evolution from mafic to syenitic magmas could not be more than 10 my.

The initial $^{87}Sr/^{86}Sr$ ratios for the mafic rocks are about 0.7051, and for the late granite pegmatites about 0.7054–0.7069. Such values are relatively low compared to most Cretaceous granites of the world's orogenic belts, but are comparable with those from the Central Asian Orogenic Belt where numerous granitoids show relatively juvenile isotopic characteristics (Kovalenko et al., 1996; Jahn et al., 2000; Heinhorst et al., 2000; Wu et al., 2000). The $\varepsilon_{Nd}(T)$ values calculated for $T = 130$ Ma range from -1.9 to -2.4 for the mafic rocks and from -2.9 to -3.5 for the syenites (Table 9). All the rocks have rather young depleted-mantle-based model ages of about 900 Ma assuming a single-stage evolution, or about 1100 Ma if a two-stage evolution is assumed (Table 9). On an $\varepsilon_{Nd}(T)$ vs. I_{Sr} plot (Fig. 13), the Oshurkovo data fall in the enriched mantle segment. However, we underline the slight but distinguishable difference in isotopic compositions of mafic and syenitic rocks. This isotopic distinction is significant, and it will be used to constrain the processes of magmatic evolution discussed below.

8. Discussion

8.1. Cumulate crystals in magmas forming the Oshurkovo Complex

A common problem in the study of plutonic rocks is the estimation of magma composition inasmuch as the bulk chemical composition of rock samples is unlikely to represent that of the magma due to crystal fractionation and accumulaton processes (Irvine, 1979; Klewin, 1990; Tommasini and Poli, 1992). The Oshurkovo Complex is exceptional by its high abundance of inclusions of mafic rocks in which the mineral assemblage Prg + Cpx + Ap makes up 70–75% of the rock and apatite alone amounts to 10–12%. This suggests that accumulation processes in the alkali mafic magma occurred widely. Chemical and mineralogical data also suggest that cumulus crystals are abundant in the plutonic mafic rocks, at least in monzodiorite. In all bivariate plots, as well as in the REE patterns (Figs. 8 and 10), the compositions of cumulates and monzodiorite overlap almost entirely. In monzodiorite, as in the blocks of cumulate, no correlation between MgO and some major oxides and trace elements (K_2O, FeO*, TiO_2, Rb, Ba) is observed; chemical compositions of amphibole from these two rock types are similar (Fig. 4). These data suggest a large amount of Prg + Cpx + Ap cumulus crystals in the monzodiorite. There is also evidence that the syenites to some extent crystallized from magma enriched in cumulus phase. The Eu/Eu* values of syenite, from 1.50 to 1.71 (Table 8), point to feldspar accumulation in the rock. In addition, the wide range of Ba and Sr in syenites within a fairly narrow interval of MgO content (Fig. 8) suggests accumulation of feldspar in the syenitic magma as well.

For estimation of the parental basic magma composition, chilled margins of plutonic bodies are commonly studied. In the Oshurkovo plutonic rocks chilled zones are absent, but they are widespread in the dike-like chilled intrusive sheets. However, in the given case, this approach seems inappropriate because most of the mafic dikes are similar in composition to mafic plutonic rocks with significant amounts of late Cpx + Bi assemblage (Fig. 9). Judging from the sub-linear arrangement of melamonzonite and monzonite compositions in bivariate plots (Fig. 8), these rocks could have crystallized from magma with minor amounts of cumulus phases. We did not find any evidence that enabled us to assess the proportion of cumulus crystals in these rocks. Because of this, the composition of the parental alkali basic magma is taken, by convention, as the average of four representative chemical analyses of melamonzonite in Table 7. As for monzonites and syenites, we assume that the most evolved varieties of these rocks correspond, as a first approximation, to composition of magmas.

8.2. Fluid content and P–T conditions of magma crystallization

The presence of a significant amount of volatiles in the magmas of the Oshurkovo Complex can be established even at the stage of field study from the abundance of pegmatite veins, segregations and clots, as well as by the predominance of amphibole and

Table 9
Rb–Sr and Sm–Nd isotope data for the Oshurkovo Complex

Sample no.	Rock type	Rock/Min.	Rb (ppm)	Sr (ppm)	$^{87}Rb/^{86}Sr$	$^{87}Sr/^{86}Sr$	$\pm 2\sigma m$	$(^{87}Sr/^{86}Sr)_i$
Analyses performed in Rennes								(130 Ma)
37-1	monzodiorite (MD)	WR	13.25	4741	0.0081	0.705135	6	0.70512
61	melamonzonite (MM)	WR	27.02	6875	0.0114	0.705160	6	0.70514
34-1	monzonite (M)	WR	9.58	6310	0.0044	0.705120	6	0.70511
1	early syenite (SY-1)	WR	66.7	8420	0.0229	0.705292	7	0.70525
9	early syenite (SY-1)	WR	41.5	7609	0.0158	0.705322	5	0.70529
65-1	late syenite (SY-2)	WR	52.4	3065	0.0495	0.705470	6	0.70538
14	late quartz syen. (QSY-2)	WR	118.6	2539	0.1349	0.705667	8	0.70542
59	monzodiorite (MD)	biotite	136.7	320.7	1.2311	0.707339	8	0.70506
		apatite	7	5800	0.0035	0.705140	5	0.70513
59-1	mafic cumulate	biotite	129.7	469.8	0.7973	0.706639	6	0.70517
		apatite	13	6900	0.0054	0.705118	9	0.70511
								(120 Ma)
153	granitic pegmatite	WR	458.2	298.7	4.43	0.713842	7	0.70628
		biotite	4849	46.88	315.1	1.249082	9	0.71171
153b	granitic pegmatite	WR	768.6	272.1	8.17	0.719129	6	0.70520
Analyses performed in Ulan Ude								(120 Ma)
151-3	granitic pegmatite	WR	186.1	667.4	0.807	0.70682	9	0.70544
		biotite	1260	42.73	86.52	0.85445	20	0.70689
152-1	granitic pegmatite	WR	373.7	351.2	3.08	0.71099	16	0.70574
153-3	granitic pegmatite	WR	503.3	303.1	4.81	0.71425	10	0.70605
	granitic pegmatite	biotite	4715	78.9	178.0	1.00692	12	0.70335
211	granitic pegmatite	WR	295.0	87.45	9.77	0.72285	12	0.70618
		biotite	2493	32.47	230.0	1.07500	18	0.68275
		garnet	4.05	17.26	0.678	0.70790	15	0.70674
79-5	monzonitic pegmatite	WR	21.15	7567	0.008	0.70540	10	0.70539

Sample no.	Rock type	Rock/Min.	Rb (ppm)	Sr (ppm)	$^{87}Rb/^{86}Sr$	$^{87}Sr/^{86}Sr$	$\pm 2\sigma m$	$(^{87}Sr/^{86}Sr)_i$
79-9	monzonitic pegmatite	WR	32.77	4310	0.022	0.70541	11	0.70537
79-2	monzonitic pegmatite	biotite	166.2	209	2.300	0.70924	13	0.70532
79-3a	monzonitic pegmatite	biotite	121.1	198	1.767	0.70863	20	0.70562
79	monzonitic pegmatite	biotite	177.1	232	2.213	0.70938	12	0.70561
79		pyroxene	2.91	448	0.019	0.70538	8	0.70535
79		apatite	2.50	6637	0.001	0.70559	8	0.70559
79-3a	monzonitic pegmatite	apatite	2.50	6320	0.012	0.70556	11	0.70554
Analyses performed at IGEM, Moscow (V. Yarmolyuk)								
Osh-1/24	amazonite pegmatite	WR	1472	71.4	60.2	0.809013	17	0.70634
Osh-1/25	granitic pegmatite	WR	62.8	322	0.564	0.706375	14	0.70541
Osh-2/18	aplite	WR	150	872	0.499	0.706306	15	0.70546

Sample no.	Rock type	Rock/Min.	Sm (ppm)	Nd (ppm)	$^{147}Sm/^{144}Nd$	$^{143}Nd/^{144}Nd$	$\pm 2\sigma m$	$\varepsilon_{Nd}(0)$	$\varepsilon_{Nd}(T)$	$f_{Sm/Nd}$	$T_{DM}-1$	$T_{DM}-2$
Analyses performed in Rennes									(130 Ma)			
37-1	monzodiorite (MD)	WR	25.11	153.1	0.0992	0.512437	5	−3.9	−2.3	−0.50	949	1117
61	melamonzonite (MM)	WR	18.04	119.1	0.0916	0.512424	5	−4.2	−2.4	−0.53	906	1127
34-1	monzonite (M)	WR	14.46	93.2	0.0938	0.512451	5	−3.6	−1.9	−0.52	889	1087
1	early syenite (SY-1)	WR	10.46	69.3	0.0912	0.512400	6	−4.6	−2.9	−0.54	933	1165
9	early syenite (SY-1)	WR	7.40	49.7	0.0900	0.512379	8	−5.1	−3.3	−0.54	950	1197
65-1	late syenite (SY-2)	WR	6.12	48.1	0.0769	0.512387	5	−4.9	−2.9	−0.61	850	1167
14	late quartz syen. (QSY-2)	WR	7.14	55.9	0.0772	0.512358	4	−5.5	−3.5	−0.61	884	1214

CHUR (chondritic uniform reservoir): $^{147}Sm/^{144}Nd = 0.1967$; $^{143}Nd/^{144}Nd = 0.512638$. Used in model age calculation, DM (depleted mantle): $^{147}Sm/^{144}Nd = 0.2137$; $^{143}Nd/^{144}Nd = 0.51315$. $T_{DM}-1 = 1/\lambda \times \ln[1+(0.51315-(^{143}Nd/^{144}Nd)s)/(0.2137-(^{147}Sm/^{144}Nd)s]$. $T_{DM}-2=[(\varepsilon_{DM}-\varepsilon_{sample}+QT_c(f_s-f_{cr})/Q(f_{DM}=f_{cr})$, where $\varepsilon_{DM}=10$, $f_{DM}=0.086$, $f_{cr}=-0.4$, and $Q=25.1$. Thus $T_{DM}-2=[(10-\varepsilon_{sample}+25.1T_c(f_s+0.4)]/[25.1(0.086+0.4)]$.

All in-run errors of isotopic ratios represent two standard errors, and correspond to the last decimal points of the reported ratios.

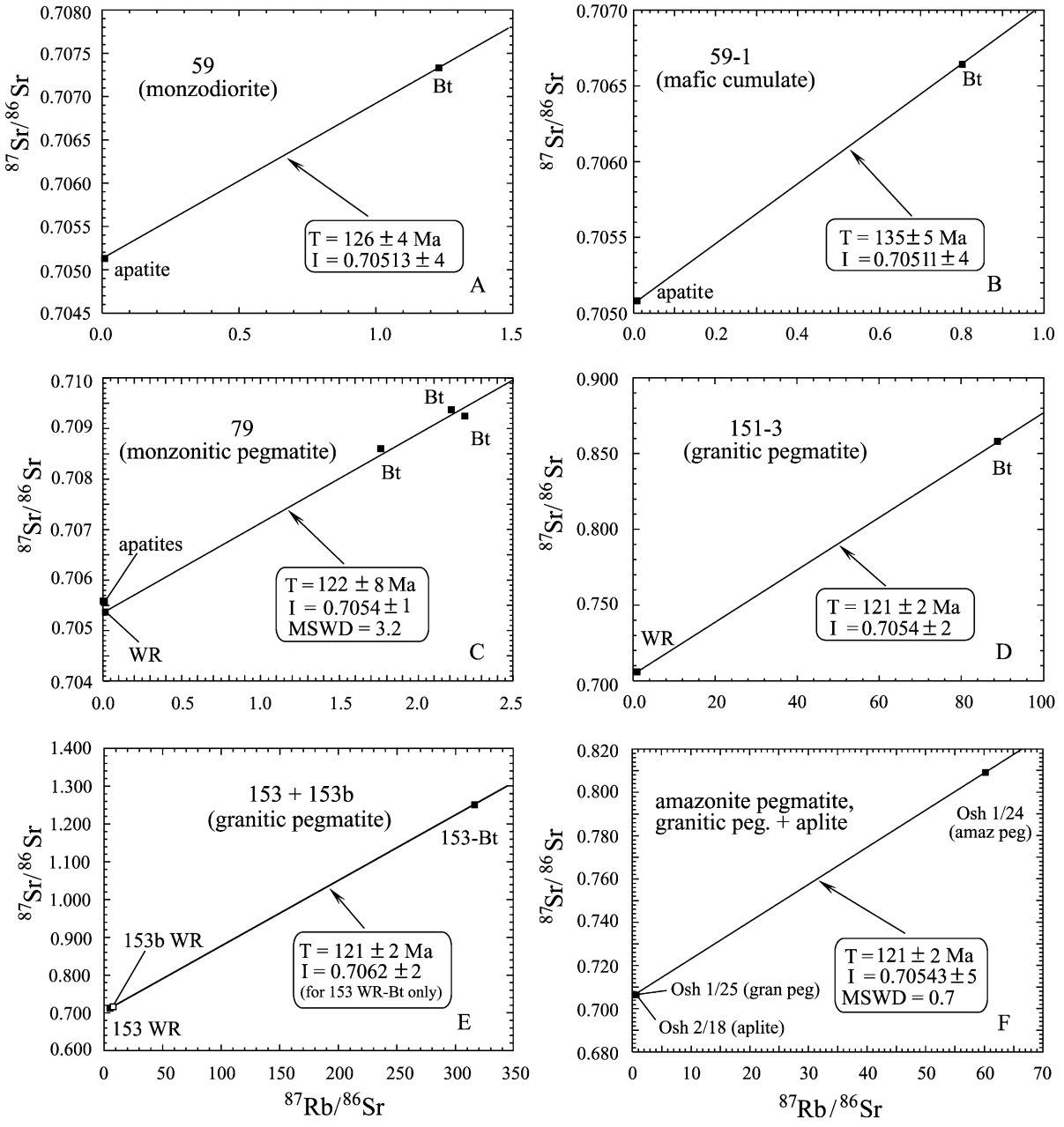

Fig. 12. Rb–Sr isochron diagrams of mafic rocks and pegmatites of the Oshurkovo Complex.

biotite among the mafic minerals. It was shown above that in most cases pargasite, kaersutite and Mg–hastingsite were liquidus minerals. According to available experimental data, early crystallization of amphibole in the absence of plagioclase points to high water content in the melt, about 4–6 wt.% at a pressure of 2 kbar (Anderson, 1980 and refrences therein; Baker and Eggler, 1983; Sisson and Grove, 1993). Plagioclase could crystallize near the liquidus only in dry (Upton, 1971) or water-deficient (≤ 3

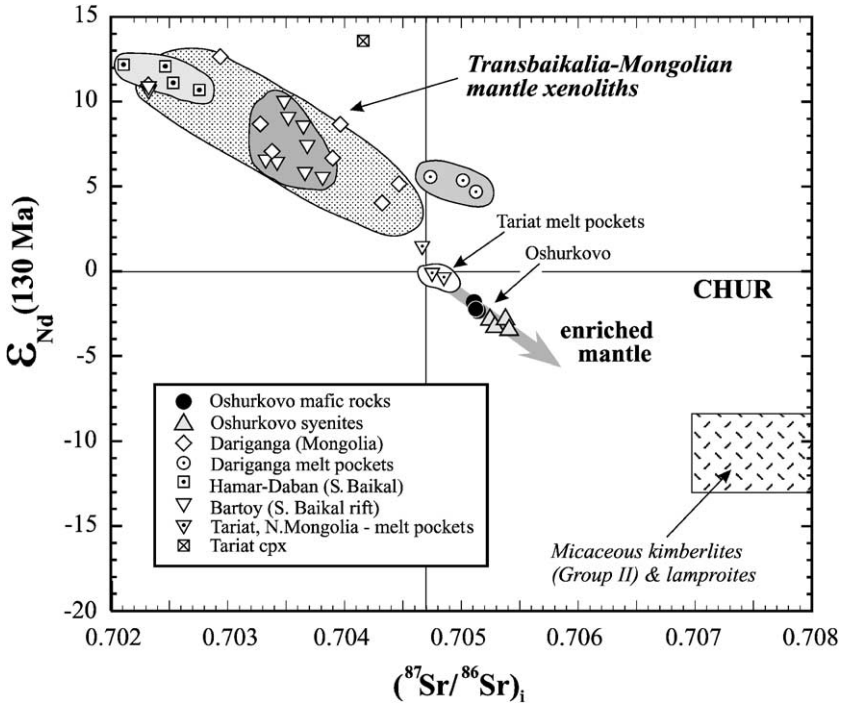

Fig. 13. $\varepsilon_{Nd}(T)$ vs. $(^{87}Sr/^{86}Sr)_i$ diagram for the rocks of the Oshurkovo Complex, age 130 Ma. Also shown are the fields of mantle xenoliths occurring in Cenozoic alkali basalts from the region of Transbaikalia and Mongolia, and the field of micaceous kimberlites and lamproites. Data sources : Wiechert et al. (1997) (Dariganga, Mongolia), Ionov et al. (1995) (Hamar-Daban, S. Baikal), Ionov et al. (1992) (Bartoy, S. Baikal), Ionov et al. (1994) (Tariat, Dariganga melt pockets, Mongolia), Menzies (1987) (micaceous kimberlites and lamproites).

wt.% H_2O) alkali basalt melt (Eggler, 1972). In addition to water, the melt was enriched in phosphorous (Table 7), and possibly in fluorine as evidenced by high fluorine concentrations in amphibole, biotite and apatite (Tables 2, 3 and 6).

The high water content in the magmas probably resulted in high oxygen fugacity. In order to estimate the oxygen fugacity during crystallization, biotites were separated and analyzed for total iron and FeO (see Section 3); the results are given in Table 3. The

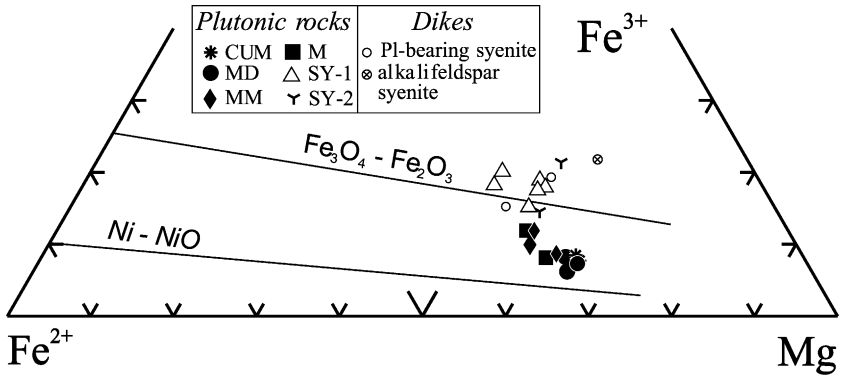

Fig. 14. Fe^{2+}–Fe^{3+}–Mg diagram for biotites illustrating changes of oxygen fugacity in the Oshurkovo rocks. The two oxygen buffers are from Wones and Eugster (1965). Symbols as in Fig. 4.

Table 10
Chemical composition (wt.%) of Fe–Ti oxides from two mafic dikes

Sample no.	31-13		52-1	
	Ilm–Mag		Ilm–Mag	
SiO_2	0.07	0.09	0.03	0.07
TiO_2	43.76	15.65	43.84	15.92
Al_2O_3	0.12	0.13	0.13	0.13
Fe_2O_3	16.55	36.46	17.5	36.4
FeO	38.88	47.13	38.11	47
MnO	0.79	0.46	1.07	0.37
MgO	0.12	0.09	0.42	0.14
CaO	0.09	0.06	0.03	0.05
Na_2O	0.09	0.04	0.15	0.13
K_2O	0.08	0.02	0.01	0.02
Total	100.55	100.13	101.29	100.23
Atoms per formula unit				
Si	0.002	0.003	0.001	0.003
Ti	0.828	0.442	0.822	0.449
Al	0.004	0.006	0.004	0.006
Fe^{3+}	0.343	1.107	0.358	1.102
Fe^{2+}	0.793	1.416	0.769	1.409
Mn	0.017	0.015	0.023	0.012
Mg	0.005	0.005	0.016	0.008
Ca	0.002	0.002	0.001	0.002
Na	0.004	0.003	0.007	0.009
K	0.003	0.001	951	0.001
log $f(O_2)$	− 10.63		− 10.44	

(1) Formula coefficients were calculated to three atoms of oxygen for ilmenite and four atoms for Ti–magnetite; Fe^{3+} was calculated by stoichiometry.
(2) Ilm–Mag = ilmenite and Ti–magnetite lamellae measured in a single grain.
(3) The oxygen fugacity was determined by the Anderson and Lindsley (1985) method.

biotite compositions in a ternary Fe^{2+}–Fe^{3+}–Mg diagram (Fig. 14) of Wones and Eugster (1965) suggest oxygen fugacities above the NNO buffer. The syenite melt crystallized at a fO_2 at or above the HM buffer. Estimates of fO_2 from the Fe–Ti oxide oxygen geobarometer (Anderson and Lindsley, 1985) are fraught with difficulties for plutonic rocks because of exsolution at low temperatures. Therefore, fO_2 values were obtained for two fine-grained monzonite dikes (Table 10); the log fO_2 values are − 10.44 and − 10.63, which at 950–960 °C corresponds to just above the NNO buffer value.

The temperatures of magma crystallization were determined using the amphibole (Otten, 1984), ternary feldspar (Lindsley and Nekvasil, 1989; Nekvasil, 1992) and Fe–Ti oxide (Anderson and Lindsley, 1985) geothermometer (Table 11). The amphibole compositions used for temperature determination are marked by superscript "T" in Table 2. The temperatures calculated for pargasite from the mafic rocks are all within a narrow range of 1006–1031 °C and must represent the near-liquidus state of the parental tephritic magma. The compositions of ternary feldspar in the Ab–An–Or diagram with isotherms (Fig. 6, Table 5) suggest that crystallization of ternary feldspar began at about 900 °C in the melamonzonite. In monzonite, this mineral crystallized at lower temperatures, 800–850 °C (Fig. 6). In the early syenite, ternary feldspar is a near-liquidus mineral. Therefore, the temperature of its crystallization of about 850 °C (Fig. 6) may characterize the near-liquidus conditions for the syenite magma. The temperatures of 950–960 °C determined for the mafic dikes using Fe–Ti oxides (Table 11) fall in the solidus-to-liquidus temperature interval for monzodiorite.

Concerning the depth of the complex formation, we have to remember that within the same tectonic block, about 30 km west of the Oshurkovo Complex, the Early Cretaceous volcanic equivalents of the plutonic rocks

Table 11
Estimates of temperatures (°C) during the crystallization of the tephritic magmas

Sample no./Min.	38	58-3	59-1	38-3	38-6	58	37-1	36-2	58-4	62	61	34-7	8	54-10	54-1	51-3	31-13	52-1
	Cumulate (CUM)				Monzodiorite (MD)				Melamonzonite (MM)					Monzonite (M)			Mafic dikes	
Amphibole	1011	1011	1009	1006	1029	1026	1019		1031	1018	1005	999						
Ternary feldspar		900–960	900	850–960	870–930	870	830–910	900	850		840	860–940	910	850	850	800		
Fe–Ti oxides																	950	961

Temperatures were calculated by amphibole (Otten, 1984), ternary feldspar (Lindsley and Nekvasil, 1989; Nekvasil, 1992), and Fe–Ti oxides (Anderson and Lindsley, 1985) geothermometers.

are abundant (Yarmolyuk et al., 1998). This suggests that erosion of the block since Cretaceous was not significant. Consequently, the complex formation occurred at shallow depth, not more than some few kilometers. The amphibole geobarometer gives a value of $\sim 6 \pm 3$ kbar (Hammarstrom and Zen, 1986). However, this pressure may represent crystallization in a deep magmatic reservoir before high-level emplacement.

Data on the enrichment of alkali mafic magma in water and other volatiles provide an explanation for specific mineral composition of mafic rocks. Due to early crystallization of pargasite and apatite, the melt became enriched in alkalis, whereas calcium decreased. As a result, plagioclase that crystallized later is impoverished in An component. Early crystallization of significant amount of Na-rich and Si-poor amphibole can account for absence of modal nepheline despite the tephritic composition of magma. Abundance of liquidus amphibole in mafic rocks suggests that alkali monzodiorite and monzonite from the Oshurkovo Complex can be considered as plutonic equivalents of lamprophyres. They are closely associated and genetically related with lamprophyric dike-like bodies (chilled intrusive sheets). By mineralogical and bulk composition, they are approximated to appinite (Rock, 1991).

8.3. Origin of the syenite magmas

The syenites in the Oshurkovo Complex are closely associated, spatially and temporally, with the alkali basic rocks. A number of geochemical, mineralogical, and isotopic characteristics suggest a close genetic link between these rock types. First of all, the concentrations of Sr and Ba are unusually high and similar in monzodiorite, monzonite and syenite of the same stage, about 6000–8000 ppm Ba and 5000–8000 ppm Sr. In addition, the SY-1 is enriched in P_2O_5, up to 1.3 wt.% (Table 7), while Rb contents, like in the mafic rocks, are low, only 30–40 ppm. Early syenites, like the mafic rocks, have nepheline in the norms and contain three feldspars, among them ternary feldspar that shows considerable compositional overlap with ternary feldspar from monzodiorite and monzonite (Figs. 6 and 7). The isotope characteristics of SY-1 and mafic rocks are similar although not identical (Table 9, Fig. 13). Lastly, similar patterns of element abundance in monzodiorite, monzonite and SY-1 (Fig. 11) also support the assumption of consanguinity between mafic and felsic rocks.

Alkali-feldspar syenites of the second stage (SY-2), in spite of rather specific mineral compositions, also exhibit evidence of a genetic relationship with the mafic rocks. This is manifested in the very high Sr and Ba contents, about 4000 and 6000 ppm, respectively, and low Rb, 70–90 ppm. Normative nepheline is not uncommon in these rocks (Table 7). The REE abundances in SY-2 are similar to those in SY-1 (Fig. 10B). $\varepsilon_{Nd}(T)$ values in SY-2 and SY-1 are identical within the error limits (Table 9).

The evidence of consanguinity between syenites and alkali-rich mafic rocks allow us to conclude that of all possible models of syenite magma generation, the *fractional crystallization model* is the most appropriate. As shown in the preceding sections, fractionation processes occurred at all stages of the monzodiorite–syenite series evolution. This is manifested in the formation of melanocratic cumulates, as well as in enrichment of cumulus crystals in monzodiorite and early syenites. It is also illustrated in Fig. 3 that even within small mafic bodies differentiation may result in appearance of leucocratic segregations of the syenite composition.

Fractional crystallization may have been accompanied by crustal assimilation. However, the SY-1 has similar Sr and even higher Ba contents than the mafic rocks (Fig. 8, Table 7), and this limits the possible amount of crustal assimilation. For instance, if we assume assimilation of the gneissic granite that makes up several large plutons near the Oshurkovo Complex (Fig. 1), a comparison of Ba and Sr contents in the gneissic granite with those of basic rocks and SY-1 shows that the proportion of the assimilant would not be significant (sample #591 in Tables 7 and 8, bivariate plots in Fig. 8). However, for SY-2 the significant role of assimilation cannot be excluded.

8.3.1. Fractional crystallization modeling

The crustal fractionation process can be modeled by least-square methods; however, because cumulate crystals are present in all rock types, the modeling provides only a crude numerical approximation. The calculations were performed based on the average composition of melamonzonite as parent and the most

evolved monzonite (sample 32-11), SY-1 (sample 9) and SY-2 (sample 33-1). In Tables 2, 5–8, samples of rocks and minerals chosen for calculation are marked by the superscript "M". Three stages of crystal fractionation were calculated: (1) formation of monzonite from melamonzonite; (2) formation of SY-1 from monzonite; (3) formation of SY-2 from SY-1.

The results of the two first calculations are presented in Table 12. It follows that monzonite could be produced from the parental magma by fractionation of amphibole with subordinate apatite and Fe–Ti oxides. The important role of amphibole among the fractionating minerals is clearly illustrated by its position in bivariate diagrams (Fig. 8). The proportion of the melt remaining is 73 wt.%. To produce a SY-1 melt from the monzonitic magma (stage 2), extraction of equal amounts of amphibole and plagioclase (in total about 33 wt.%), minor apatite and Fe–Ti oxides is necessary. For both stages the proportion of minerals fractionated seems realistic, considering the modal mineral compositions of mafic rocks and SY-1 (Table 1). The trace and rare-earth element test also gave a satisfactory match between the calculated and observed values in daughter melts for all elements, except for Sr, as well as Tb and Yb in stage 2.

To obtain the SY-2 daughter melt from the SY-1 magma, we performed calculations for all possible

Table 12
Results of least-squares modelling of the monzonite magma fractional crystallization

	Stage 1: melamonzonite–monzonite			Stage 2: monzonite–SY-1		
	Parent	Daughter		Parent	Daughter	
	Average ($n=4$)	Observed #32-11	Calculated	#32-11	Observed #9	Calculated
SiO_2	48.07	54.34	53.75	54.34	57.67	57.19
TiO_2	2.97	1.64	1.63	1.64	1.40	1.33
Al_2O_3	16.32	18.20	18.89	18.20	18.69	19.03
FeO	10.10	7.00	6.96	7.00	5.38	5.35
MnO	0.08	0.05	0.04	0.05	0.04	0.00
MgO	4.93	3.25	3.45	3.25	2.01	2.25
CaO	8.17	5.49	5.47	5.49	3.72	3.57
Na_2O	4.38	5.36	5.27	5.36	5.40	5.38
K_2O	3.01	3.69	3.58	3.69	5.06	5.11
P_2O_5	1.97	0.99	0.96	0.99	0.61	0.79
Rb	19	24	24	24	46	34
Ba	5175	5300	6311	5300	7000	6937
Sr	7125	6500	8423	6500	8050	6427
La	88	60.5	58	60.5	45	60
Ce	240	117.4	142	117.4	98	107
Nd	140	71.9	74	71.9	52	59
Sm	18	11.5	9	11.5	6.2	8.8
Eu	5.4	4.2	3	4.2	2.9	3.2
Tb	1.2	0.95	0.6	0.95	0.36	0.76
Yb	0.8	0.45	0.6	0.45	0.29	0.42
Fractionating	Amphibole		21.3			16.6
minerals, wt.%	Apatite		3			1.1
	Fe–Ti oxides		2.7			0.9
	Plagioclase		–			16.5
Residual melt, wt.%			73.0			64.8
Sum residuals squared			0.788			0.342

(1) Major elements are recalculated to total = 100% volatile free; total Fe as FeO.
(2) Mineral compositions used for modelling are marked with superscript "M" in Tables 2, 5 and 6.
(3) Sources of partition coefficients values. *Amphibole*: Arth (1976) (Rb, Ba, Sr) and Fujimaki (1984).
Plagioclase: Lamarchand et al. (1987) (Rb, Ba, Sr) and Luhr et al. (1984). Fe–Ti oxides: Luhr et al. (1984). Apatite: Luhr et al. (1984) and Feeley and Davidson (1994) (Rb, Ba); K^D Sr (0.6) is calculated by the authors using the content of Sr in the apatite phenocrysts and in the matrix from the lamprophyre dikes of the Oshurkovo Complex.

mineral assemblages, but even in the best version the value of sum residuals squared is 5.17 (not shown in Table 12). This suggests that the SY-2 was not produced by fractional crystallization alone. At first glance, formation of SY-2 can be easily explained by admixture of granitic material to the SY-1 magma (see sample 591 in Tables 7 and 8). However, this model looks feasible only for quartz-bearing varieties of SY-2 because for this rock it is supported by isotope data (Table 9). As for the dominating quartz-free variety of SY-2, its isotope characteristics, $\varepsilon_{Nd}(T)$ and $(^{87}Sr/^{86}Sr)_i$, are indistinguishable from that of SY-1.

We believe that fluid mass-transport could have occurred at this stage in the evolution. It follows from Table 12 that the SY-1 residuum at stage 2 constitutes about 50% of the parental melamonzonite melt. If the H_2O content in the parental basic magma was about 4–5% (see above), the syenite residuum could contain up to 8–9 wt.% H_2O. This value is above the upper limit of H_2O solubility in silicic magmas at 2–3 kbar (Johannes and Holtz, 1996; Holloway and Blank, 1994), and therefore a significant amount of exsolved fluid phase could co-exist with the syenitic magma at this stage of evolution. It was shown by Webster et al. (1998) that H_2O and F rich fluids can dissolve more than 10 wt.% of major and trace elements even at 2 kbar pressure. If this is the case, fluids could transport significant amounts of major and trace elements and cause their redistribution. The appearance of monzonitic pegmatite veins with inner zones of syenitic composition (Table 7) could be considered as indirect evidence for the operation of these processes.

8.3.2. AFC modeling

Although fractional crystallization is considered as the predominant process for the Oshurkovo magmatic evolution, the Nd–Sr isotopic data reveal an noticeable role of crustal contamintion in the generation of syenitic magmas, particularly for quartz-bearing varieties of SY-2 (Table 9). The Sr–Nd isotopic data for all monzodioritic rocks are identical within the error limits (Table 9), hence we interpret that the magmatic evolution within this rock group has followed essentially a closed system fractional crystallization. However, the clear distinction in isotopic composition between the mafic rocks and the syenites (Fig. 13) suggests an open system process. In order to examine this problem, a modelling study was performed assuming concurrent crustal assimilation and fractional crystallization (AFC process, De Paolo, 1981).

In the modelling the following assumptions were made: (1) the rate of assimilation to the rate of crystallization (parameter r = Ma/Mc) varies from 0.1 to 0.5. The high value of 0.5 is considered possible in view of the high magmatic temperatures (ca. 1000 °C) and enhanced H_2O content in mafic magma; (2) the bulk distribution coefficients (D) for Sr and Nd were estimated from the least-square modelling of crystallization and the known mineral-melt partition coefficients (Table 12); and (3) the two end-members are represented by an average melamonzonite and an average continental upper crust, of which the Sr–Nd isotopic and concentration data are given in the caption of Fig. 15. We performed the modelling for Nd–Sr isotope shift as well as for the change of Ba and Sr concentrations, which are unusually high for magmatic rocks, but quite sensitive to crustal contamination.

The results of the model calculations are presented in Fig. 15. In Fig. 15A, three curves are shown to indicate the isotopic trends with varying r proportion. The value of each tick represents the amount of residual magma (F). For a small ratio of assimilation to crystallization (r = 0.1), it would require a very advanced AFC (F about 0.2) to achieve the isotope shift from monzodiorite to syenite. This is considered unlikely because the Ba–Sr concentration data as shown in Fig. 15B limit the residual magma to be about 60%. If r = 0.3 is considered, then both the Nd–Sr isotope and Ba–Sr concentration data would meet the constraint. Furthermore, Fig. 15B indicates that the very high r value of 0.5 would severely reduce Sr concentration from 7000 to 4000 ppm when residual magma would be reduced to 60%. This is not compatible with the analytical data for the SY-1 system, but is possible for the alkali feldspar syenites (SY-2). Though the modelling does not produce a perfect fit for all isotopic and elemental data, it seems reasonable to conclude that during the differentiation about 10–20% of crustal mass could be assimilated to produce syenitic magmas when 30–50% of the solid was fractionated (F = 65–50%). Such a high amount of crustal contamination can be understood when the Sr isotopic composition of ca. 0.7051 in the mafic rocks of very high Sr concentrations (5000–9000 ppm) is to

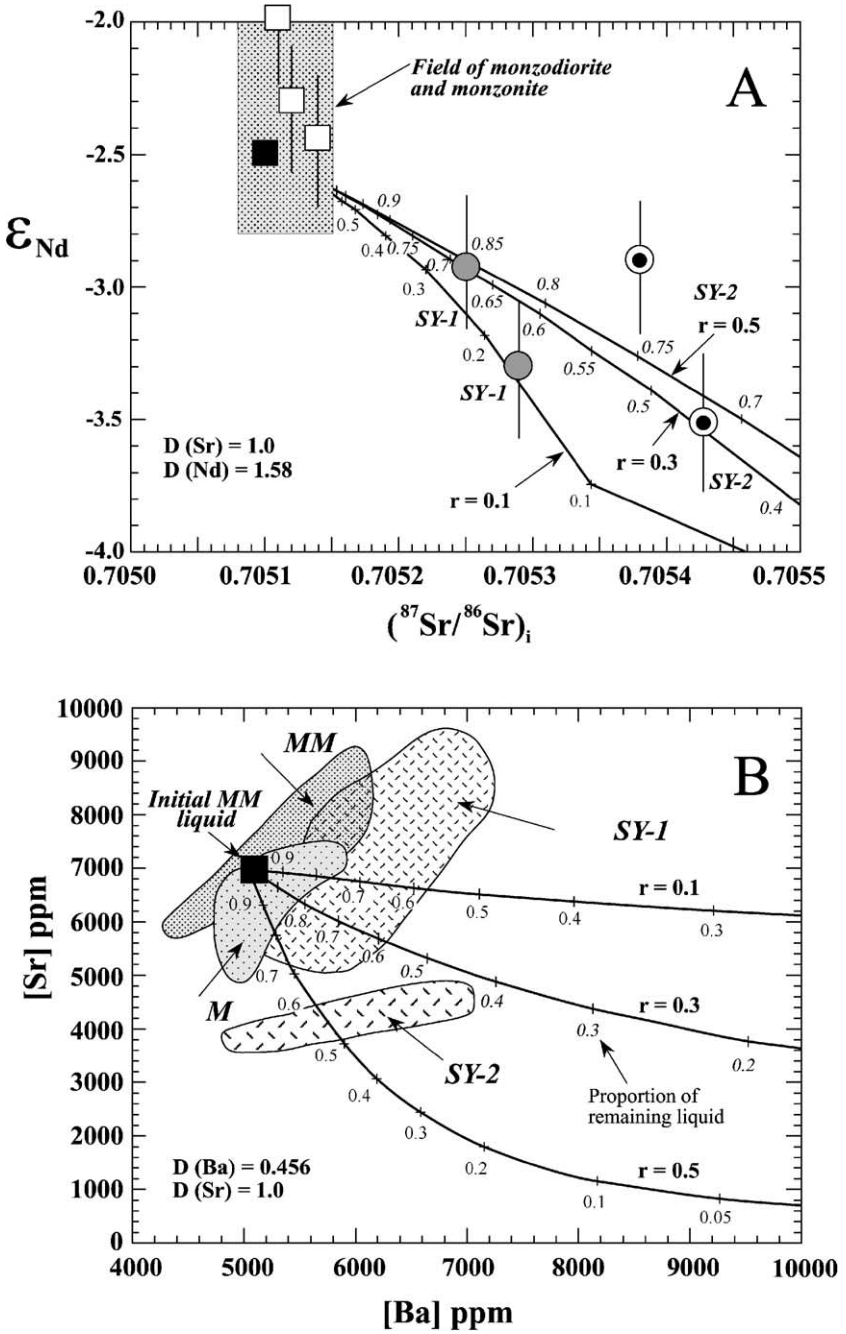

Fig. 15. AFC modelling showing (A) trends of Nd–Sr isotope variation as a result of crystallization–assimilation under upper crustal condition, and (B) trends of Sr and Ba concentration variation in the same process. The parameters used in the modelling are as follows: Initial magma (melamonzonite): [Ba] = 5000 ppm, [Sr] = 7000 ppm, [Nd] = 90 ppm, $^{87}Sr/^{86}Sr = 0.7051$, $\varepsilon_{Nd} = -2.5$. Country rock (assimilant): [Ba] = 800 ppm, [Sr] = 400 ppm, [Nd] = 26 ppm, $^{87}Sr/^{86}Sr = 0.7200$, $\varepsilon_{Nd} = -10$. The concentration data represent the highest estimates from the literature. They are chosen to show the maximum effect of crustal contamination.

be shifted to about 0.7053 (SY-1) or 0.7054 (quartz-bearing SY-2).

Thus, the isotope data, unlike the chemical data, enable us to estimate the amount of crustal material that could be assimilated in the course of tephrite magma evolution. However, both approaches demonstrate that the dominant process in the monzodiorite–syenite series formation was fractional crystallization of alkali mafic magmas. The fact that the Oshurkovo Complex formed by numerous injections of tephritic, tephro-phonolitic and syenitic batches of magma (plutonic sheeted complex) suggests that the fractional crystallization process occurred at a depth that was much greater than the depth of the complex. The pressures estimated from amphibole geobarometers (6 ± 3 kbar) may point to magma evolution in a reservoir at a depth of 10–20 km. The parental tephrite magma, in its turn, could have formed at still greater depth by fractional crystallization of a more primitive mantle-derived magma.

8.4. Provenance of tephrite magmas from the Oshurkovo Complex

The tephrite magma that formed the Oshurkovo Complex is characterized by large negative Nb and Zr anomalies (Fig. 11). This is quite unusual for magmas of this type. Such anomalies are commonly observed in the continental crust or crustal-derived granitoids. Their appearance in mafic rocks is often attributed to crustal contamination during magma differentiation. However, the case for the Oshurkovo rocks is more complicated.

It was noted earlier that in the Early Cretaceous, simultaneously with emplacement of the Oshurkovo tephrite magmas, abundant K-rich basalts, tephrites, phonolites and trachytes were extruded over the whole territory of Western Transbaikalia (Yarmolyuk et al., 1998). High Sr, Ba, and P, Sr–Nd isotope ratios similar to those of the Oshurkovo rocks, as well as negative Nb anomalies in tephrites, are characteristic of these volcanic rocks. It is notable that in all Phanerozoic volcanic series of Transbaikalia, phosphorus enrichment (1.5–2 wt.%) is observed only in basalt–tephrite series of the Late Jurassic–Cretaceous stage. Thus, during a single magmatic stage, large volumes of mafic magma with specific chemical and isotope compositions were generated. The negative $\varepsilon_{Nd}(T)$ values for the melamonzonite, basalts and tephrites with very high Nd concentrations (100–150 ppm) could not have been produced by any reasonable amount of crustal contamination, if the source rocks are ordinary mantle peridotites. The Cretaceous stage of magmatic activity was typically within-plate, and ocean plate subduction had ceased still in the Middle Paleozoic. We consider it is most likely that the negative $\varepsilon_{Nd}(T)$ and high $(^{87}Sr/^{86}Sr)_i$ values and negative Nb anomalies in the spidergrams of the Oshurkovo Complex were caused by melting of metasomatised mantle. The metasomatism could be produced by interaction of lithospheric mantle with slab-derived fluids during an earlier phase of subduction, as proposed by Tatsumi et al. (1986) and Mc Culloch and Gamble (1991). Similar hypothesis was suggested for the Pliocene–Pleistocene basanites and alkali basalts from the Iblea area, Sicily (Beccaluva et al., 1998). Unlike the Oshurkovo mafic melts, magmas from Sicily were poorly differentiated and contained less water and phosphorus.

In Fig. 13, we have compiled the available data for mantle xenoliths in Cenozoic alkali basalts from Transbaikalia and Mongolia (Ionov et al., 1992, 1994, 1995; Wiechert et al., 1997). Though many of them show petrographic and chemical evidence of metasomatic effects, all the isotopic data fall in the depleted mantle quadrangle except two melt pockets from Tariat, Northern Mongolia. Clearly, the metasomatism in these xenoliths must have occurred not long before the partial melting events. In the Oshurkovo case, the mantle source was likely enriched much earlier. Because partial melt (basaltic liquid) tends to have a lower Sm/Nd ratio than the source peridotite, the calculated single-stage model ages (ca. 900 Ma, Table 9) set the minimum age for the metasomatic event. Nb and Zr were not enriched because of their immobility or insolubility in the slab fluids, whereas the LILE were highly concentrated, particularly Ba and Sr. Note that Yarmolyuk et al. (1998) also proposed metasomatism to explain the elemental enrichment in alkali basalts and tephrites of Transbaikalia, which is not as spectacular as in the Oshurkovo alkali mafic rocks. Thus, it is likely that Cretaceous mafic magmatism in Transbaikalia provides evidence for long-term (Late Proterozoic) mantle metasomatism which is not reflected by Cenozoic mantle xenolith data.

9. Conclusions

(1) The rocks of the Oshurkovo Complex form a continuous series ranging from alkali monzodiorite to syenite. The Complex was emplaced in the Cretaceous (~ 130 Ma) by numerous injections of tephritic, phono-tephritic and syenitic magmas into an expanding system of sub-parallel and near-vertical fissures in a plutonic sheeted complex.

(2) The mafic magma was enriched in water (≥ 4–6%), phosphorous (about 2 wt.%) and probably fluorine. Due to high volatile and phosphorous contents, its liquidus temperature was only slightly higher than 1000 °C.

(3) Monzodiorite and monzonite of the Oshurkovo Complex can be considered as plutonic equivalents of lamprophyres and approximate to appinite.

(4) The alkali monzodiorite–syenite series was produced mainly by fractional crystallization of amphibole, apatite, Fe–Ti oxides and later plagioclase from parental tephritic magma. The syenitic magma formed at a temperature of ~ 850 °C after fractionation of about 50% of crystals from the parental mafic liquid. The entire magmatic differentiation was completed within ≤ 10 my, as inferred from numerous cross-cutting granite pegmatites, all dated at about 120 Ma.

(5) Nd–Sr isotope data indicate that assimilation of crustal rocks took place concurrently with fractional crystallisation. AFC modeling suggests 10–20% of crustal rocks had to be assimilated to explain the isotopic difference between monzonites and syenites.

(6) The mantle source rocks were enriched, particularly in Sr, Ba, P and LREE, by metasomatism in the Precambrian.

Acknowledgements

The authors are grateful to L.M. Larsen and B. Robins for thoughtful revision of the manuscript and valuable suggestions that provided more clear and correct presentation. Also we are indebted to K.P. Skjerlie, M.P. Roberts, M. Wilson and Bin Chen for their important comments. This work was supported by Russian Foundation of Basic Researches (RFBR), grants #99-05-65138 (to BAL), #97-05-963555 (to ANZ), #01-05-97255 (to MGSh). BmJ acknowledges the financial support of the French INSU-CNRS through programs "Dynamique des Transferts Terrestres 1997" and "Intérieur de la Terre 1999" for study of Phanerozoic crustal growth in Central Asia. This is also a contribution to project IGCP-420.

References

Allen, C.M., Chappell, B.W., 1992. Association of I-type granites with rift related alkalic magmatism in central coastal Queensland, Australia. Geol. Soc. Am. Abstr. Programs 24, 43.

Anderson, A.T., 1980. Significance of hornblende in calc-alkaline andesites and basalts. Am. Mineral. 65, 837–851.

Anderson, D.J., Lindsley, D.H., 1985. New (and final!) models for the Ti-magnetite/Ilmenite geothermometer and oxygen barometer. EOS Trans. 66, 416.

Arth, J.G., 1976. Behaviour of trace elements during magmatic processes — a summary of theoretical models and their applications. J. Res. U. S. Geol. Surv. 4, 41–47.

Baker, D.R., Eggler, D.H., 1983. Fractionation paths of Atka (Aleutians) high-alumina basalts: constraints from phase relations. J. Volcanol. Geotherm. Res. 18, 387–404.

Barker, F., Wones, D.R., Sharp, W.N., Desborough, G.A., 1975. The Pikes Peak batholith, Colorado Front Range, and a model for the origin of the gabbro–anorthosite–syenite–potassic granite suite. Precambr. Res. 2, 97–160.

Beccaluva, L., Siena, Ff., Coltorti, M., Grande, A.D.I., Lo Giudice, A., Macciotta, G., Tassinari, R., Vavvaro, C., 1998. Nephelinic to tholeiitic magma generation in the transtensional tectonic setting: an integrated model of the Iblean volcanism, Sicily. J. Petrol. 39, 1547–1576.

Brown, P.E., Becker, S.M., 1986. Fractionation, hybridisation and magma-mixing in the Kialineq centre East Greenland. Contrib. Mineral. Petrol. 92, 57–70.

De Paolo, D.J., 1981. Trace element and isotopic effects of combined wall-rock assimilation and fractional crystallization. Earth Planet. Sci. Lett. 53, 189–202.

Deer, W.A., Howie, R.A., Zussman, J., 1978. Rock Forming Minerals. Single-Chain Silicates, vol. 2A. Wiley, New York.

Dorais, M.J., 1990. Compositional variations in pyroxenes and amphiboles of the Belknap Mountain complex, New Hampshire: evidence for origin of silica-saturated alkaline rocks. Am. Miner. 75, 1092–1105.

Eggler, D.H., 1972. Water-saturated and undersaturated melting reaction in a Paricutin andesite and an estimate of water content in the natural basalt magma. Contrib. Mineral. Petrol. 34, 261–271.

Faure, G., 1986. Principles of Isotope Geology, 2nd ed. Wiley, New York.

Feeley, T.C., Davidson, P., 1994. Petrology of calc-alkaline lavas at volcan Ollague and the origin if compositional diversity at Central Andean stratovolcanoes. J. Petrol. 35, 1295–1340.

Fujimaki, H., 1984. Partition coefficients of Hf, Zr and REE between zircon, apatite and liquid. Contrib. Mineral. Petrol. 94, 42–45.

Hammarstrom, J.M., Zen, E., 1986. Aluminum in hornblende: an empirical igneous geobarometer. Am. Mineral. 71, 1297–1313.

Heinhorst, J., Lehmann, B., Ermolov, P., Serykh, V., Zhurutin, S., 2000. Paleozoic crustal growth and metallogeny of Central Asia: evidence from magmatic–hydrothermal ore system of Central Kazakhstan. Tectonophysics 328, 69–87.

Holloway, J.R., Blank, J.G., 1994. Application of experimental results to C–O–H species in natural melts. In: Carrol, M.R., Hollowey, J.R. (Eds.), Reviews in Mineralogy, vol. 30. Mineral. Soc. America, Washington, DC, pp. 187–227.

Huang, W.L., Wyllie, P.J., 1981. Phase relationships of S-type granite with H2O to 35 kbar: muscovite granite from Harney Peak, South Dakota. J. Geophys. Res 86, 10515–10529.

Ionov, D.A., Kramm, U., Stosch, H.G., 1992. Evolution of the upper mantle beneath the southern Baikal rift zone: an Sr–Nd isotope study of xenoliths from the Bartoy volcanoes. Contrib. Mineral. Petrol. 111, 235–247.

Ionov, D.A., Hofmann, A.W., Shimizu, N., 1994. Metasomatism-induced melting in mantle xenoliths from Mongolia. J. Petrol. 35, 753–785.

Ionov, D.A., O'Reilly, S.Y., Ashchepkov, I.V., 1995. Feldspar-bearing lherzolite xenoliths in alkali basalts from Hamar-Daban, southern Baikal region, Russia. Contrib. Mineral. Petrol. 122, 174–190.

Irvine, T.N., 1979. Rocks whose composition is determined by crystal accumulation and sorting. In: Yoder, H.S. (Ed.), The Evolution of Igneous Rocks. Princeton Univ. Press, Princeton, NJ, pp. 245–306.

Jäger, E., Niggli, E., Wenk, E., 1967. Rb–Sr Altersbestimmungen an Glimmern der Zentralalpen. Beitr. Geol. Kt. Schweiz NF 134, 1–67. Bern.

Jahn, B.M., Cornichet, J., Cong, B.L., Yui, T.F., 1996. Ultrahigh-ε_{Nd} eclogites from an ultrahigh-pressure metamorphic terrane of China. Chem. Geol. 127, 61–79.

Jahn, B.M, Wu, F.Y., Chen, B., 2000. Massive granitoid generation in central Asia: Nd isotopic evidence and implication for continental growth in the Phanerozoic. Episodes 23, 82–92.

Jenkin, G.R.T., Ellam, R.M., Rogers, G., Stuart, F.M., 2001. An investigation of closure temperature of the biotite Rb–Sr system: the importance of cation exchange. Geochim. Cosmochim. Acta 65, 1141–1160.

Johannes, W., Holtz, F., 1996. Petrogenesis and Experimental Petrology of Granite Rocks. Springer-Verlag, Berlin.

Klewin, K.W., 1990. Petrology of the Proterozoic Potato River layered intrusion, Northern Wisconsin, USA. J. Petrol. 31, 1115–1139.

Kovalenko, V.I., Yarmolyuk, V.V., Kovach, V.P., Kotov, A.B., Kozakov, I.K., Sal'nikova, E.B., 1996. Sources of Phanerozoic granitoids in Central Asia: Sm–Nd isotope data. Geochem. Int. 34, 628–640.

Kretz, R., 1983. Symbols for rock-forming minerals. Am. Mineral. 68 (1–2), 277–279.

Kuznetsov, A.N., 1980. Mineralogy and Geochemistry of Apatite-bearing Diorites Nauka, Novosibirsk (in Russian).

Lamarchand, F., Villemant, B., Calas, G., 1987. Trace element distribution coefficients in alkaline series. Geochim. Cosmochim. Acta 51, 1071–1082.

Leake, B.E., 1978. Nomenclature of amphiboles. Am. Mineral 63, 1023–1053.

Le Maitre, R.W., 1976. The chemical variability of some common igneous rocks. J. Petrol. 17, 589–637.

Lindsley, D.H., Nekvasil, H., 1989. A ternary feldspar model for all reasons. EOS Trans. Am. Geophys. Union 70, 506.

Litvinovsky, B.A., Zanvilevich, A.N., Posokhov, V.F., Vrublevskaya, T.T., Burdukov, I.V., 1998. New data of the structure and age of the Oshurkovo pluton of alkaline gabbro and syenites, Transbaikalia. Russ. Geol. Geophys. 39, 727–741.

Litvinovsky, B.A., Zanvilevich, A.N., Wickham, S.M., Steele, I.M., 1999. Origin of syenitic magmas from anorogenic granitoid series: syenite–granitic series from Transbaikalia. Petrology 7, 483–508.

Lubala, R.T., Frick, C., Roders, J.H., Walraven, F., 1994. Petrogenesis of syenites and granites of the Schiel Alkaline complex, Northern Transvaal, South Africa. J. Geol. 102, 307–309.

Ludwig, K.R., 1999. ISOPLOT/Ex. Version 2.06. A geochronological toolkit for Microsoft Excel. Berkeley Geochronology Center Sp. Publ., vol. 1a, 49 pp.

Luhr, J.F., Carmichael, I.S.E., Varekamp, J.C., 1984. The 1982 eruption of El Chichon volcano, Chiapas, Mexico: mineralogy and petrology of the anhydrite-bearing pumices. J. Volcanol. Geotherm. Res. 23, 69–108.

Lynch, D.J., Musselman, T.E., Gutmann, J.T., Patchett, P.J., 1993. Isotopic evidence for the origin of Cenozoic volcanic rocks in the Pinacate volcanic field, northwestern Mexico. Lithos 29, 295–302.

Mc Culloch, M.T., Gamble, J.A., 1991. Geochemical and geodynamical constraints on subduction zone magmatism. Earth Planet. Sci. Lett. 102, 358–374.

Menzies, M., 1987. Alkaline rocks and their inclusions : a window on the Earth's interior. In: Fitton, J.G., Upton, B.G.J. (Eds.), Alkaline Igneous Rocks. Geol. Soc. Spec. Publ., vol. 30, pp. 15–27.

Nekvasil, H., 1992. Feldspar crystallisation in felsic magmas: a review. Spec. Pap. Geol. Soc. Am. 272, 399–407.

Otten, M.T., 1984. The origin of brown hornblende in the Artfjallet gabbro and dolerites. Contrib. Mineral. Petrol. 86, 189–199.

Parker, D.F., 1983. Origin of the trachyte–quartz trachyte–peralkalic rhyolite suite of the Oligocene Paisano volcano, Trana-Pecos Texas. Geol. Soc. Am. Bull. 94, 614–629.

Reid Jr., J.B., Hamilton, M.A., 1987. Origin of Sierra Nevada Granite : evidence from small scale composite dikes. Contrib. Mineral. Petrol. 96, 441–454.

Ribbe, P.H., 1983. Exolution textures in ternary and plagioclase feldspars; interference colors. In: Ribbe, P.H. (Ed.), Feldspar Mineralogy. Rev. Mineral., Mineral. Soc. Am., vol. 2, pp. 241–270.

Rieder, M., Cavazzini, G., D'Yakonov, Yu.S., Frank-Kamenetsky, V.A., Gattardi, G., Guggenheim, S., Koval, P.V., Müller, G., Neiva, A.M., Radaslovich, E.W., Robert, J.-L., Sassi, F.P., Takeda, H., Weiss, Z., Wones, D.R., 1999. Nomenclature of the micas. Mineral. Mag. 63, 267–279.

Rock, N.M.S., 1991. Lamprophyres. Blackie and Son, Glasgow.

Sheppard, S., 1995. Hybridization of shoshonitic lamprophyre and calc-alkaline granite magma in the Early Proterozoic Mt. Bundey igneous suite, Northern Territory. Aust. J. Earth Sci. 42, 173–185.

Sisson, T.W., Grove, T.L., 1993. Experimental investigations of the role of H2O in calc-alkaline differentiation and subduction zone magmatism. Contrib. Mineral. Petrol. 113, 143–166.

Smith, J.V., Brown, W.L., 1988. Feldspar Minerals: 1. Crystal Structures, Physical, Chemical, and Microtextural Properties. Springer-Verlag, Berlin.

Sun, S.-S., Mc Donough, W.F., 1989. Chemical and isotopic systematics of oceanic basalts: implications for mantle compositions and processes. In: Saunders, A.D., Norry, M.J. (Eds.), Magmatism in the Ocean Basins. Geol. Soc. Spec. Publ., vol. 42, pp. 313–345.

Sutcliffe, R.H., Smith, A.R., Doherty, W., Barnett, R.L., 1990. Mantle derivation of Archean amphibole-bearing granitoids and associated mafic rocks: evidence from the southern Superior Province, Canada. Contrib. Mineral. Petrol. 105, 255–274.

Tatsumi, Y., Hamilton, D.L., Nesbitt, R.W., 1986. Chemical characteristics of fluid phase from a subducted lithosphere and roigin of arc magmas: evidence from high-pressure experiments and natural rocks. J. Volcanol. Geotherm. Res. 29, 293–309.

Thorpe, R.S., Tindle, A.G., 1992. Petrology and petrogenesis of a Tertiary bimodal dolerite–peralkaline/subalkaline trachyte/rhyolite dyke association from Lundy, Bristol Channel. U. K. Geol. J.V. 27, 101–117.

Tommasini, S., Poli, G., 1992. Petrology of the late-Carboniferous Punta Falcone gabroic complex, northern Sardinia, Italy. Contrib. Mineral. Petrol. 110, 16–32.

Upton, B.G.J., 1971. Melting experiments on chilled gabbros and syenogabbros. Yearb Carnegie Inst. Washington 70, 112–118.

Vogel, T.A., Wilband, J.T., 1978. Coexisting acidic and basic melts: geochemistry of a composite dike. J. Geol. 86, 353–371.

Webster, J.D., Thomas, R., Veksler, I., Rhede, D., Seltman, R., 1998. Late-stage processes in P- or F-rich granitic magmas. Acta Univ. Carol., Geol. 42, 181–188.

Wickham, S.M., Litvinovsky, B.A., Zanvilevich, A.N., Bindeman, I.N., 1995. Geochemical evolution of Phanerozoic magmatism in Transbaikalia, East Asia: a key constraint on the origin of K-rich silicic magmas and the process of cratonization. J. Geophys. Res. 100/B8, 15641–15654.

Wiebe, R.A., 1973. Relations between coexisting basaltic and granitic magmas in a composite dike. Am. J. Sci. 273, 130–151.

Wiechert, U., Ionov, D.A., Wedepohl, K.H., 1997. Spinel peridotite xenoliths from the Atsagin-Dush volcano, Dariganga lava plateau, Mongolia: a record of partial melting and cryptic metasomatism in the upper mantle. Contrib. Mineral. Petrol. 126, 345–364.

Wones, D.R., Eugster, H.P., 1965. Stability of biotite: experiment, theory and applications. Am. Mineral 50, 1228–1272.

Wu, F.Y., Jahn, B.M., Wilde, S., Sun, D.Y., 2000. Phanerozoic continental crustal growth: Sr–Nd isotopic evidence from the granites in northeastern China. Tectonophysics 328, 89–113.

Yarmolyuk, V.V., Kovalenko, V.I., Ivanov, V.G., 1995. Late Mesozoic–Cenozoic intraplate volcanic province of Central Eastern Asia; projection of mantle hot field. Geotektonika 5, 41–67 (in Russian).

Yarmolyuk, V.V., Ivanov, V.G., Kovalenko, V.I., 1998. Sources of intraplate magmatism of western Transbaikalia in the Late Mesozoic–Cenozoic: trace element and isotope data. Petrology 6, 101–123.

Zanvilevich, A.N., Litvinovsky, B.A., Andreev, G.V., 1985. Mongolian–Transbaikalian alkaline granitoid province Nauka, Moskow (in Russian).

Zhao, J.-X., Shiraishi, K., Ellis, D.J., Sheraton, J.W., 1995. Geochemical and isotopic studies of syenites from the Yamoto Mountains, East Antarctica : Implication for the origin of syenitic magmas. Geochim. Cosmochim. Acta 59, 1363–1385.